NASA CR-135210

COMBUSTION OF LIQUID SPRAYS AT HIGH PRESSURES

by

A. J. Shearer and G. M. Faeth

Mechanical Engineering Department
The Pennsylvania State University
University Park, Pennsylvania

prepared for

NATIONAL AERONAUTICS AND SPACE ADMINISTRATION

NASA Lewis Research Center
Contract NGR 39-009-077
Richard J. Priem, Program Manager and Technical Monitor

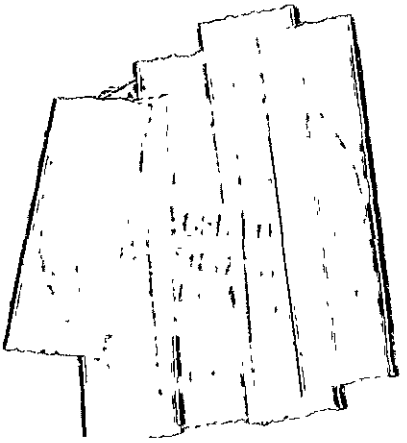

NOTICE

This work was prepared as an account of Government sponsored work. Neither the United States, nor the National Aeronautics and Space Administration (NASA), nor any person acting on behalf of NASA:

A) Makes any warranty or representation, expressed or implied, with respect to the accuracy, completeness, or usefulness of the information contained in this report, or that the use of any information, apparatus, method, or process disclosed in this report may not infringe privately owned rights; or

B) Assumes any liabilities with respect to the use of, or for damages resulting from the use of any information, apparatus, method or process disclosed in this report.

As used above, "person acting on behalf of NASA" includes any employee or contractor of NASA, or employee of such contractor, to the extent that such employee or contractor of NASA, or employee of such contractor prepares, disseminates, or provides access to, any information pursuant to his employment or contract with NASA, or his employment with such contractor.

1. Report No.	2 Government Accession No	3 Recipient's Catalog No
NASA CR - 135210		

4. Title and Subtitle	5. Report Date
Combustion of Liquid Sprays at High Pressures	March, 1977
	6. Performing Organization Code

7. Author(s)	8. Performing Organization Report No.
A. J. Shearer and G. M. Faeth	
	10 Work Unit No

9. Performing Organization Name and Address	11. Contract or Grant No.
Mechanical Engineering Department The Pennsylvania State University University Park, Pennsylvania 16802	NGR 39-009-077
	13. Type of Report and Period Covered
12. Sponsoring Agency Name and Address	Annual Report for 1976
National Aeronautics and Space Administration Washington, D. C. 20546	14. Sponsoring Agency Code

15. Supplementary Notes

Project Manager, Richard J. Priem, Chemical Propulsion Division
NASA Lewis Research Center, Cleveland, Ohio

16. Abstract

The combustion of pressure atomized fuel sprays in high pressure stagnant air was studied. Measurements were made of flame and spray boundaries at pressures in the range 0.1-9 MPa for methanol and n-pentane. At the higher test pressure levels, critical phenomena are important. The experiments are compared with theoretical predictions based on a locally homogeneous two-phase flow model. The theory correctly predicted the trends of the data, but underestimates flame and spray boundaries by 30-50 percent, indicating that slip is still important for the present experiments (Sauter mean diameters of 30 μm at atmospheric pressure under cold flow conditions). Since the sprays are shorter at high pressures, slip effects are still important even though the density ratio of the phases approach one another as the droplets heat up. The model indicates the presence of a region where condensed water is present within the spray and provides a convenient means of treating supercritical phenomena.

17. Key Words (Suggested by Author(s))	18. Distribution Statement
Liquid Spray Combustion High Pressure Combustion	Unclassified - Unlimited

19 Security Classif. (of this report)	20 Security Classif. (of this page)	21. No of Pages	22. Price*
Unclassified	Unclassified	76	

* For sale by the National Technical Information Service, Springfield, Virginia 22161

COMBUSTION OF LIQUID SPRAYS AT HIGH PRESSURES

Summary

This report discusses activities under NASA Contract NGR 39-009-077 for the period January 1, 1976, to December 31, 1976. During this period the combustion of fuel sprays in a stagnant environment was considered both theoretically and experimentally. The work included operating conditions where liquid fuel approached its thermodynamic critical point during combustion.

The experiments considered methanol and n-pentane as fuels, injected through a single-hole, orifice-type injector into pure air. Test pressures were in the range 0.1 - 9 MPa. Measurements were made of spray and flame boundaries. The experiments were compared with theoretical predictions based on a locally homogeneous two-phase flow model. The turbulence characteristics of the jet were represented by an integral model, using a variable density entrainment law which had been developed for gas-gas and gas-liquid jet processes. The theory had not previously been compared with sprays. Aside from spray and flame boundaries, the model estimates profiles of mean quantities within the spray.

The theory correctly predicted the trends of the data, but generally underestimated the extent of the spray and flame boundaries by 30 - 50 percent. The results indicate that slip effects were still important for the present experiments (the Sauter mean diameters of the sprays were approximately 30 μm at atmospheric pressure under cold flow conditions). The accuracy of the predictions is poorer at high pressures, even though the density ratio of the two phases approaches unity, which should improve

the locally homogeneous flow approximation. The sprays are shorter at high pressures, however, and significant slip effects near the injector appear to override the density ratio effect.

The predictions indicate regions within the spray where water vapor produced by combustion should condense, however, the condensed water boundary always fell within the spray boundary for the present test conditions. Both theory and experiment did not indicate any unusual phenomena when spray gasification was completed by the fuel passing through its thermodynamic critical point.

The locally homogeneous model developed in this study is convenient to use and requires a minimum amount of input data. Quantitative accuracy could be improved by adjusting empirical parameters in the model from the values that were optimized for gas-gas and gas-liquid jets, however, further data over a wider range of injector conditions would be desirable prior to such recorrelation.

ACKNOWLEDGMENTS

The financial support of the National Aeronautics and Space Administration under Grant Number NGR 39-009-077, with Dr. R. J. Priem of the Lewis Research Center serving as contract monitor, is also gratefully acknowledged.

TABLE OF CONTENTS

TABLE OF CONTENTS (CONTINUED)

LIST OF TABLES

LIST OF FIGURES

LIST OF FIGURES (CONTINUED)

NOMENCLATURE

Symbol

a	characteristic radial length scale
A	constant used in Equation (3.42)
b	radial length scale
B	constant used in Equation (3.42)
B_g	driving potential for evaporation
B_r	driving potential for reaction
c	stoichiometric mass coefficient
c_m	spreading coefficient
c_p	specific heat
C	constant used in Equation (3.42)
d	diameter
E	entrainment constant
f	generalized similarity function
h	absolute enthalpy
Δh	enthalpy decrement
h_f	enthalpy of formation
I_i	integral constant, Equation (3.14)
K	spreading rate constant
L	combustion or evaporation length
$\dot{m}$	mass rate of flow
$\dot{M}$	momentum rate of flow
P	absolute pressure
r	radial position

NOMENCLATURE (Continued)

Symbol

T	temperature
u	axial velocity
v	radial velocity
w	mass rate of reaction
W	molecular weight
y	mass fraction
Δy	Shvab-Zeldovich variable
z	axial position
ε	empirical unmixedness parameter
η	similarity variable
ν	stoichiometric molar coefficient
ρ	density
Φ	parameter defined by Equation (3.27)

Subscripts

c	boundary condition
CO_2	carbon dioxide
f	flame
F	fuel
g	evaporating jet
G	gas
L	liquid
N_2	nitrogen
OX	oxidizer

NOMENCLATURE (Continued)

Subscripts

s	spray
W	water
o	injector exit condition
∞	infinity

ABSTRACT

The combustion of a liquid fuel spray produced by a plain orifice pressure atomized injector was considered. Combustion was examined in a stagnant air environment at pressures of .1-9 MPa for n-pentane and methanol. The higher pressure levels are in excess of the critical pressure of the fuels. Measurements of spray and flame boundaries were compared with predictions based on a locally homogeneous model of the flow which had been developed for turbulent gas-gas and gas-liquid jets. The theory correctly predicted the trends of the data, but underestimated the extent of the spray and flame boundaries by 30-50 percent. The results indicate that slip is important for the sprays considered in this investigation (cold flow Sauter mean diameters were approximately 30 μm). No unusual effects were observed for supercritical conditions. A region where water vapor produced by combustion should condense was found theoretically, however, the water condensation region fell within the spray boundaries for the present test conditions.

CHAPTER I

INTRODUCTION

1.1 General Statement of the Problem

Many important combustion systems such as liquid propellant rocket engines, diesel engines and gas turbines depend upon the spray combustion process. Modern design of combustion devices has emphasized liquid fuel combustion at high pressures often approaching the critical point of many fuels. Therefore an understanding of the spray combustion at near critical conditions would provide a useful design tool for combustion chamber development.

The spray combustion process consists of a liquid fuel flowing into a gaseous environment and reacting with the surrounding gas. Figure 1 illustrates the regions present in a spray combustion process as well as typical velocity and concentration profiles. All of the injected liquid is contained within the spray boundary. Within this region the liquid jet leaving the injector breaks up into droplets. The droplets are heated by the gas in the region and evaporate supplying gaseous fuel. The fuel is then transported toward the reaction zone by turbulent mixing. The reaction zone is a region where the oxygen and the fuel are present and the chemical reaction occurs. The reaction zone is defined by the position where the mean oxygen concentration goes to zero on the inside and where the mean fuel concentration vanishes on the outside. Combustion products produced in the reaction zone are mixed throughout the flow.

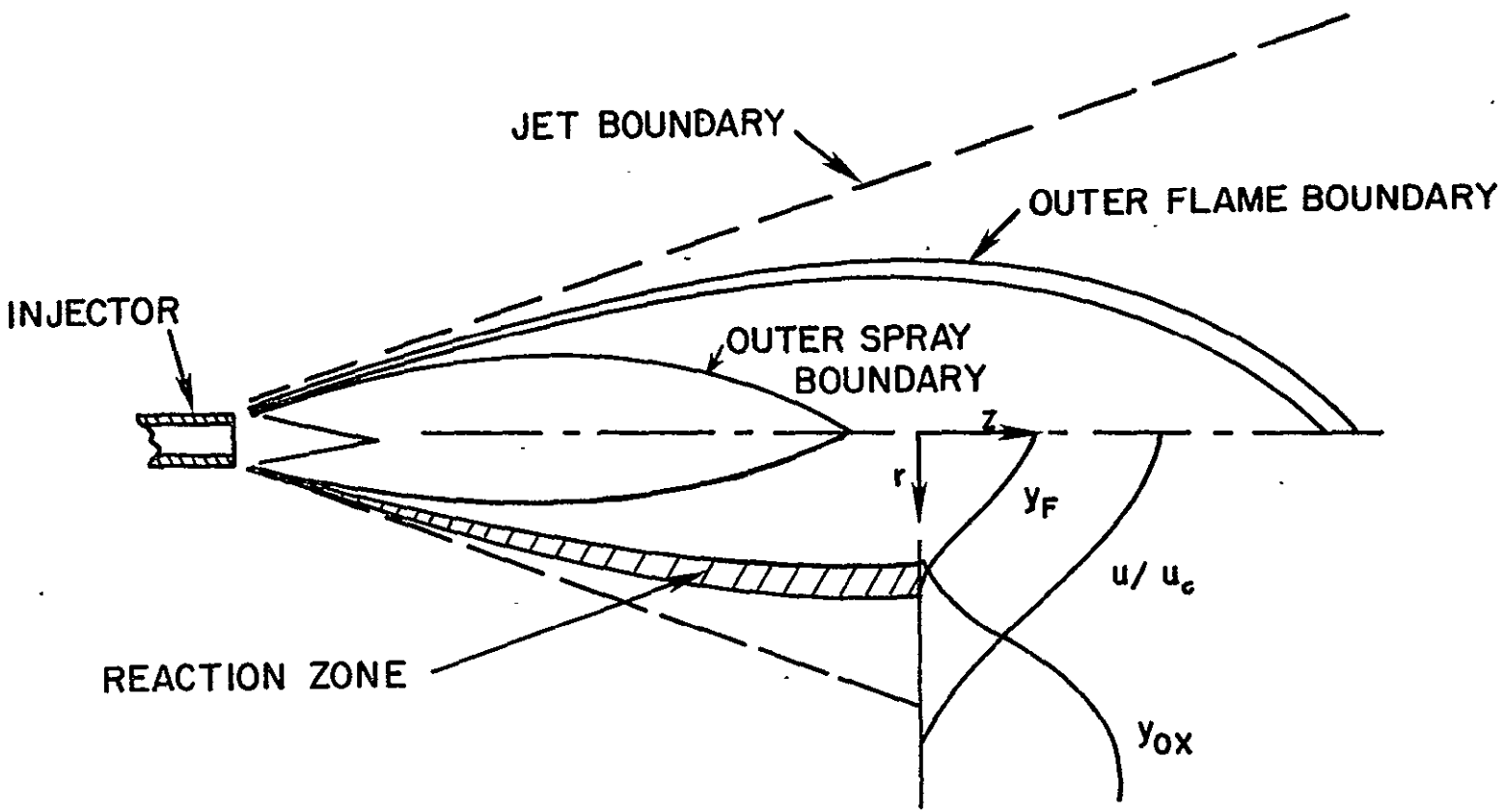

Figure 1 Sketch of the Spray Combustion Process

In order for the jet to spread, additional fluid is added to the flow by an entrainment process. Oxygen and all nonreactive gases are added to the flow in the same ratio as they present in the surrounding fluid. The jet boundary identifies the outer region of the flow where the velocity goes to zero.

The typical variation of the centerline temperature is shown in Figure 2. The centerline temperature remains relatively low in the region where drops are present. The droplets gasify by a conventional evaporation process at low pressures; at high pressures gasification can occur by the drops exceeding their thermodynamic critical point. The centerline temperature increases from the spray tip toward the reaction zone where a maximum value is reached. As additional fluid is drawn into the flow, the temperature decreases downstream of the flame tip, similar to processes occurring in a nonreactive jet.

The present study concentrated on examining the spray combustion process at elevated pressure conditions typical of spray combustion devices. The spray boundaries and the flame shape were determined for several fuels at near critical and supercritical conditions.

1.2 Previous Related Studies

The combustion of a liquid fuel spray is a complex phenomenon requiring knowledge of the evaporation and combustion processes. Individual droplet combustion has already been considered in some detail (1-4). These studies have provided the basis for predicting gasification rates typical of spray combustion systems.

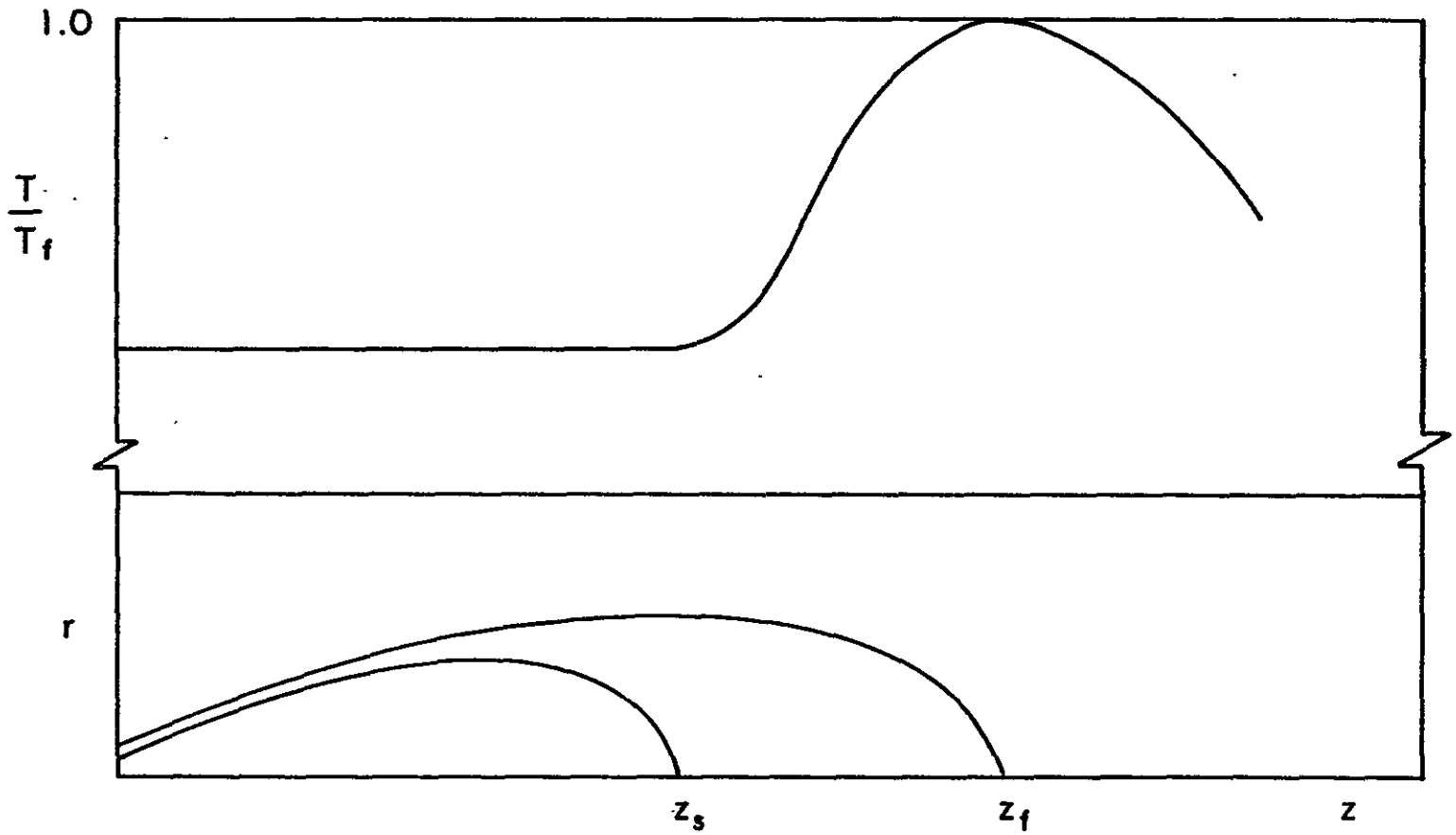

Figure 2 Centerline Temperature Variation

In order to utilize the individual droplet studies, the structure of the spray must be identified to specify the local environment of the droplets. Only recently have investigations of the spray structure during combustion appeared due to the experimental difficulty of this type of study. However, the study of some nonreacting sprays provides some insight into the two-phase nature of the spray combustion process.

Hetsroni and Sokolov (5) investigated the effect of very small liquid droplets on the structure of turbulent air jets. The droplet distribution and velocity profiles were measured and correlated with a Gaussian distribution. It was concluded that the velocity profiles of single-phase and two-phase jets were similar.

Weimer, Faeth and Olson (6) demonstrated that two-phase turbulent jets of gases into liquids may be modeled together irrespective of the vapor liquid system. Vapor penetration lengths for condensing water, ethylene glycol and iso-octane jets were correlated using a variable density single-fluid model for the two-phase flow and a variable density entrainment law to account for the turbulent mixing of the injected fluid and the surroundings. Results from Kerney, et al., (7), for condensing steam-water jets, were also correlated by the variable density model.

Tross (8) experimentally investigated a turbulent two-phase air-water jet. It was concluded that the velocity, void fraction and momentum flux possessed similar profile distributions at any position in the flow when the ratio of these quantities to their centerline values was plotted against a nondimensional radial coordinate. Gaussian distributions were shown to fit these profiles.

The characteristics of nonreacting diesel fuel sprays were experimentally investigated by Wakuri, et al., (9). Photographic measurements of fuel sprays were recorded using a high-speed motion picture camera. Nondimensional correlations were developed for spray length as functions of density ratio, inlet velocity, initial diameter and time. It was concluded that for well-atomized sprays there was negligible relative velocity between the droplets and the surrounding fluid and the two phases could be treated as a homogeneous mixture.

Newman and Brzustowski (10) investigated the behavior of a turbulent two-phase jet near the critical region of the injection fluid. Liquid carbon dioxide was injected into stagnant gaseous atmospheres of carbon dioxide and nitrogen. The two-phase spray was treated as a homogeneous turbulent jet by assuming that the droplets moved at the same velocity as the surrounding gas and were in thermal equilibrium with the gas. Success of the model was limited to order of magnitude predictions on the size of the spray boundary.

Similarities also exist between two-phase reacting sprays and single-phase reacting jets. Thring and Newby (11) analyzed the spray combustion process by burning atomized oil jets. The combustion length of the oil jets was primarily governed by the effectiveness of the mixing process. It was shown that the mixing process for two-phase jets could be adequately described by a mixing model developed for nonreacting flows.

Further investigations of the spray combustion process have been performed under atmospheric pressure conditions by Chigier and

coworkers (12, 13) and Onuma and Ogasawara (14). In these investigations, the spray structure was defined by measuring gas temperatures, droplet sizes, velocities and concentrations using air atomizing nozzles. The studies indicate that droplets in a flame do not burn individually but that the fuel vapor diffuses from the region of drop evaporation and burns like a gaseous diffusion flame.

Khalil and Whitelaw (15) also investigated the two-phase spray combustion process, but found somewhat different results. Experimental values of velocity, turbulence intensity, temperature and droplet concentration were determined for a hollow cone kerosene spray at atmospheric pressure. The flame length increased significantly when the Sauter mean diameter of the spray was increased from 45 μm to simulated gaseous diffusion flame which predicted more rapid development of the flame. This suggests that the assumption of locally homogeneous flow, which does not provide for drop size effects, can be invalid even for sprays having a Sauter mean diameter as small as 45 μm.

Avery and Faeth (16) investigated a much different problem involving the combustion of a gaseous oxidizer jet into a liquid metal fuel. The relative velocity between the two phases is small because of the relatively low inertia of the gas compared to the liquid fuel. Density variations were handled by a coordinate transformation reducing the system to the case of an incompressible jet. A unified correlation of flame length, temperatures, and velocities was developed for both the two-phase system and earlier studies of single-phase reacting jets. Figure 3 presents an example of the flame

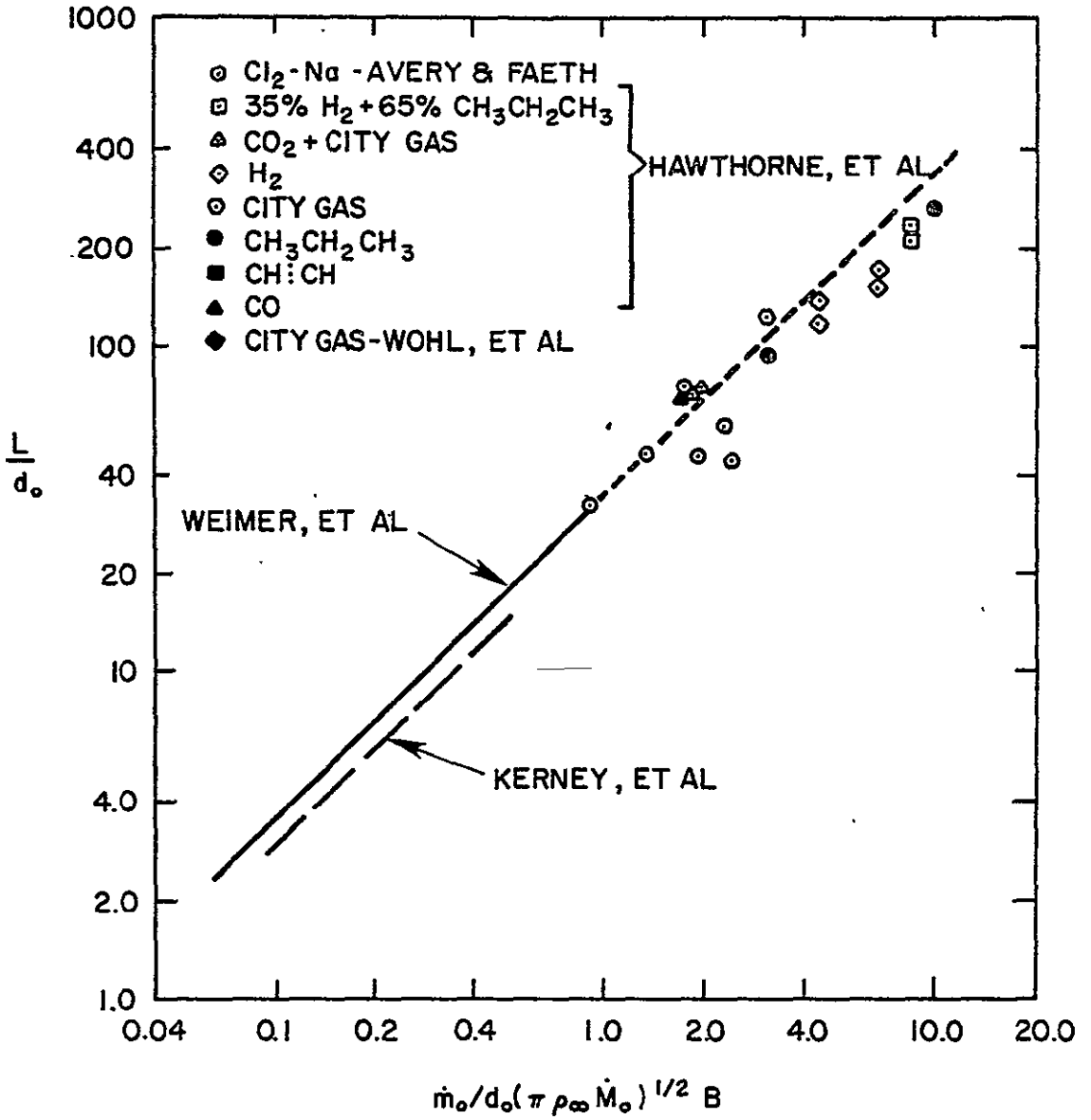

Figure 3 Comparison of Predicted and Measured Penetration Lengths for Gas-Liquid and Gas-Gas Turbulent Jets, Reference (16)

length results. The gas-liquid system of Reference (16) was compared with the gas-gas results of Hawthorne, et al., (17) and Wohl, et al., (18). It was also possible to correlate the measurements of condensing vapor jets, as shown in Figure 3.

Under the proper conditions the structure of two-phase turbulent jets are similar to single-phase jets and more importantly two-phase spray combustion processes are similar to gaseous diffusion flames. This is particularly the case when the droplets are small enough that slip between the two phases is negligible.

1.3 Specific Statement of the Problem

The preceding discussion has indicated that although some work has been done on the structure of the two-phase turbulent spray combustion processes, few studies have examined the spray combustion process at elevated pressures. Under these conditions the density variation between the liquid and gaseous phases becomes small, implying a closer approximation to the no-slip model.

The present study will examine the injection of a liquid fuel spray from a single-hole orifice-type injector, without any swirl, issuing into a stagnant environment of pure air. With this in mind the objectives of the present study are as follows:

1) Experimentally determine the spray boundary of a two-phase nonreacting liquid fuel jet.
2) Experimentally determine the spray boundary and the flame shape of a reacting two-phase turbulent jet.
3) Compare the predictions of the two-phase spray combustion model proposed by Avery and Faeth (16) to the experimental

results for reacting and nonreacting liquid fuel sprays.

CHAPTER II

EXPERIMENTAL APPARATUS AND PROCEDURE

2.1 Description of the High Pressure Experimental Apparatus

The general purpose of the experimental apparatus was to provide a large quiescent high-pressure environment for observation of the fuel spray. High-speed photographs of the spray were taken at several axial locations to form a complete picture of the spray. The photographs were used to determine the spray boundaries and flame shapes. A schematic representation of the overall experimental apparatus is illustrated in Figure 4 and a photograph of the facility is shown in Figure 5.

The test chamber consists of a 9000 cm^3 cylindrical vessel 66 cm long with an internal diameter of 13 cm. Maximum working pressure of the chamber was limited to 10 MPa. The vessel was constructed from low carbon steel which necessitated coating the interior surfaces with a rust-inhibiting paint to prevent corrosion by the combustion products. The test section of the chamber was located in the upper portion of the vessel in order to maintain the tip of the flame as far as possible from the end of the chamber. Photographic observation of the fuel spray was performed through two quartz windows approximately 1.25 cm in diameter located on opposite sides of the vessel. Visual observation of the spray was conducted through a third quartz window.

Compressed air for the experimental apparatus was supplied by a reciprocating type Ingersol Rand Compressor capable of supplying air

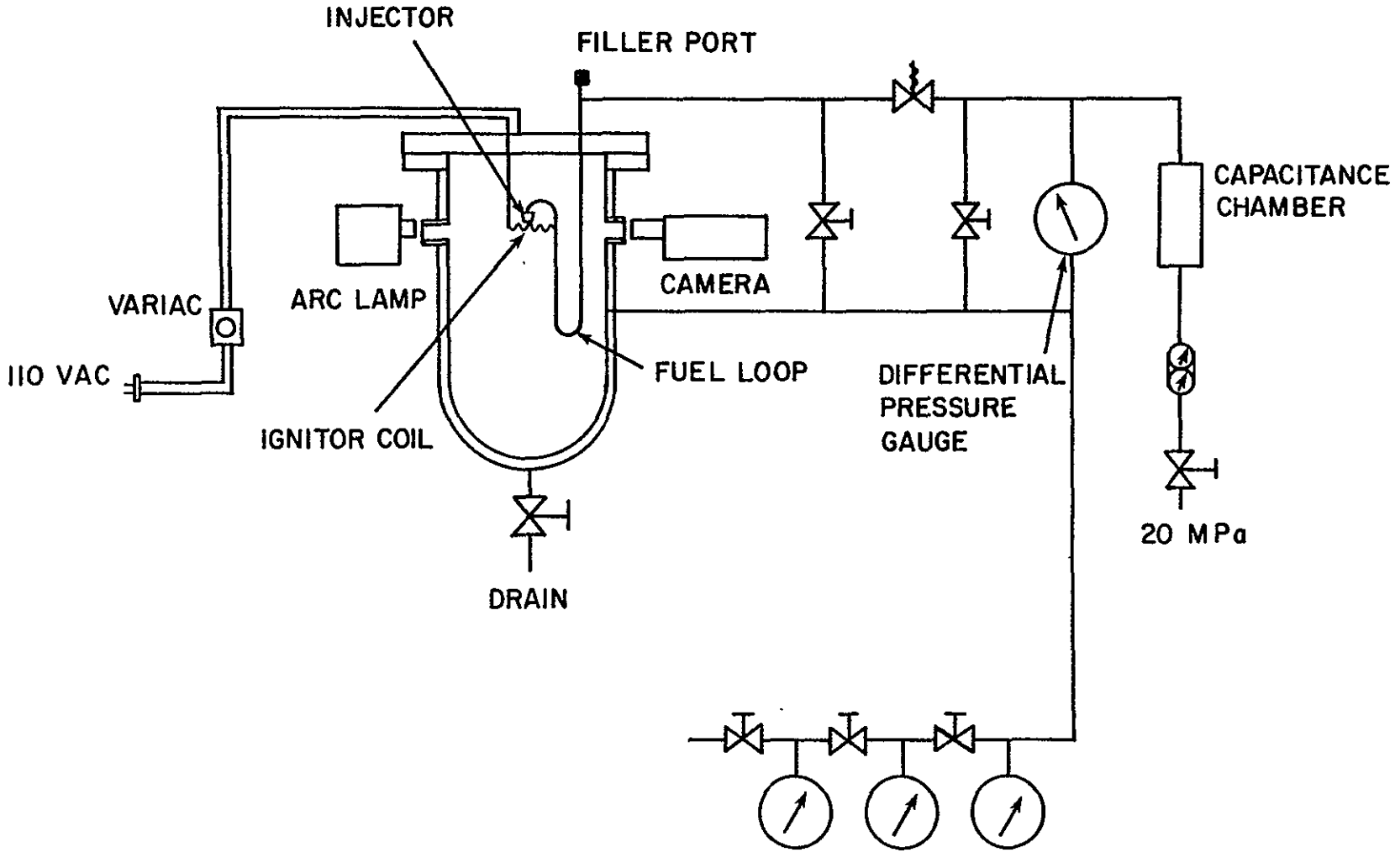

Figure 4 Sketch of the High Pressure Apparatus

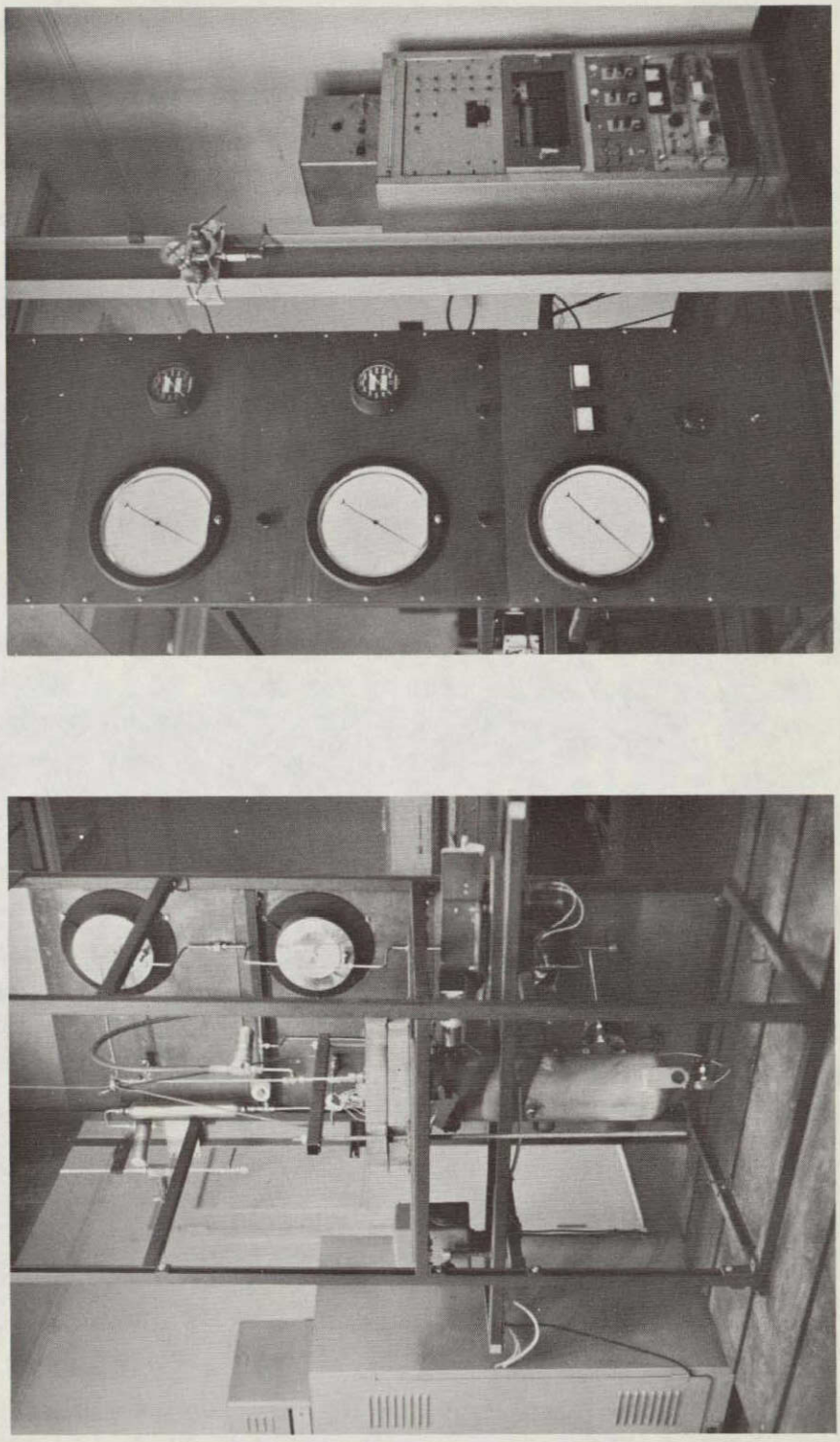

Figure 5 Photograph of the Test Facility

up to 20 MPa. The compressed air was filtered at two locations by Matheson type 451 and 453 filters to remove oil, water, or other impurities to the 5 μm level. Chamber pressure was monitored by one of three Heise pressure gages depending on the operating pressure. The three pressure ranges were 7500, 1500 and 300 psi with a specified accuracy of 7.5, 1.5 and .3 psi, respectively.

A sketch of the fuel injection assembly is shown in Figure 6. The assembly consists of a fuel loop, nozzle, nichrome igniter coil and alignment supports. The loop configuration was selected to store the fuel in order to maintain a continuous fuel slug prior to injection. Fabrication of the loop used one-quarter inch stainless steel tubing. The nozzle used throughout the tests was a stainless steel straight hole type injector, model .000009 solid stream tip, supplied by Spraying Systems Company. Attachment of the nozzle to the fuel loop was accomplished by welding the nozzle to a one-quarter inch Swagelok union which was connected to the fuel loop. The position of the nozzle was checked prior to each test by examining the fuel injection assembly through the camera eyesight. The alignment supports were also used to position the ignitor coil.

Injection of fuel into the chamber was accomplished by applying a differential pressure across the fuel loop forcing the fuel slug through the nozzle. The driving pressure was adjusted by a gas regulator and monitored by a differential pressure gage comparing the driving pressure to the chamber pressure. A solenoid valve was located upstream of the fuel loop in order to rapidly apply the driving pressure for injection. A 500 ml capacitance chamber was

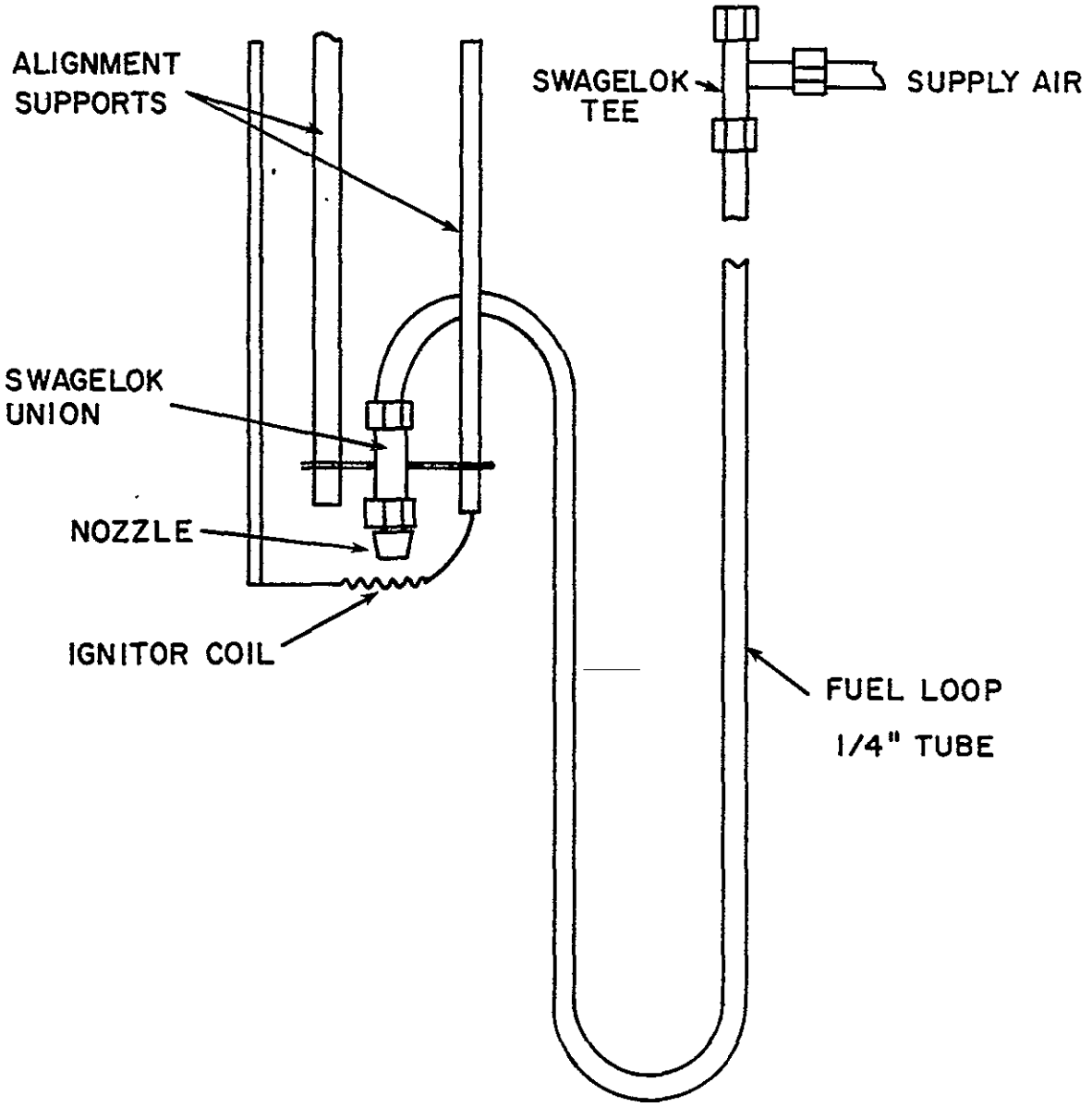

Figure 6 Sketch of the Fuel Injection Assembly

located in series with the solenoid valve in order to maintain the driving pressure relatively constant during the injection process. The test procedure was designed to use only a small amount of fuel in order to avoid large changes in the chamber pressure, temperature, and gas composition during a test. The total quantity of fuel injected was limited to 4 ml for all tests.

Ignition of the fuel spray was accomplished by positioning a heated coil of nichrome wire near the fuel spray. The coil was approximately 2.5 cm long and 0.5 cm in diameter constructed from 28 gage wire. The power input to the coil was regulated by a variable transformer and increased until the coil began to glow red. Examination of dark field photographs of the near injector region confirmed that the flame was attached back to the nozzle.

Photographic measurements of the fuel spray were recorded with a Photosonic 1-B motion picture camera using a Kepco SM36-5 AM d.c. power supply. The film speed was indicated by a timing light on the camera activated by a Wollensak Pulse generator, model 3106A, set at 100 pulses/s. Backlighting for the shadowgraph spray measurements was supplied by a Pek, model 401A arc lamp using a 75 watt mercury bulb. The light was focused into a parallel beam using the optics located in the arc lamp. A diffuser screen was used to equalize the intensity of the light beam. Kodak plus-X reversal film was used for all photographs.

The entire injection process was controlled by a mechanical timer. At the beginning of the timing cycle the electrically driven motion picture camera and pulse generator were activated and the

camera was permitted to reach operating speed. The solenoid valve was then actuated driving the fuel into the chamber. Injection continued for approximately 3 seconds before the solenoid valve was closed. The camera power and timing light generator were then turned off to complete the test cycle.

2.2 Description of the Low Pressure Experimental Apparatus

The purpose of the low pressure apparatus was to measure the flame boundaries at atmospheric conditions. A sketch of the apparatus is shown in Figure 7. The fuel injection and ignition systems were identical to those used in the high pressure tests with the exception that the nozzle was oriented horizontally. Photographs of the spray were recorded with a Graphlex camera. Polaroid type 57 film was used in these tests.

2.3 Description of the Experimental Procedure

The present investigation considered both methanol and n-pentane fuel sprays at ambient pressures of .1, 3, 6 and 9 MPa. The fuel used was of certified grade supplied by Fisher Scientific Company with a minimum purity of 98 percent for the pentane and 99.9 percent for the methanol. The temperature of the high pressure environment and liquid fuel was taken to be at room temperature which varied from 20°C to 30°C. Spray boundaries were recorded for both the reacting and nonreacting sprays along with the flame boundaries for the reacting spray.

The field of view consisted of an area approximately 1.25 cm^2. Because the fuel spray was longer than the field of view, the injector

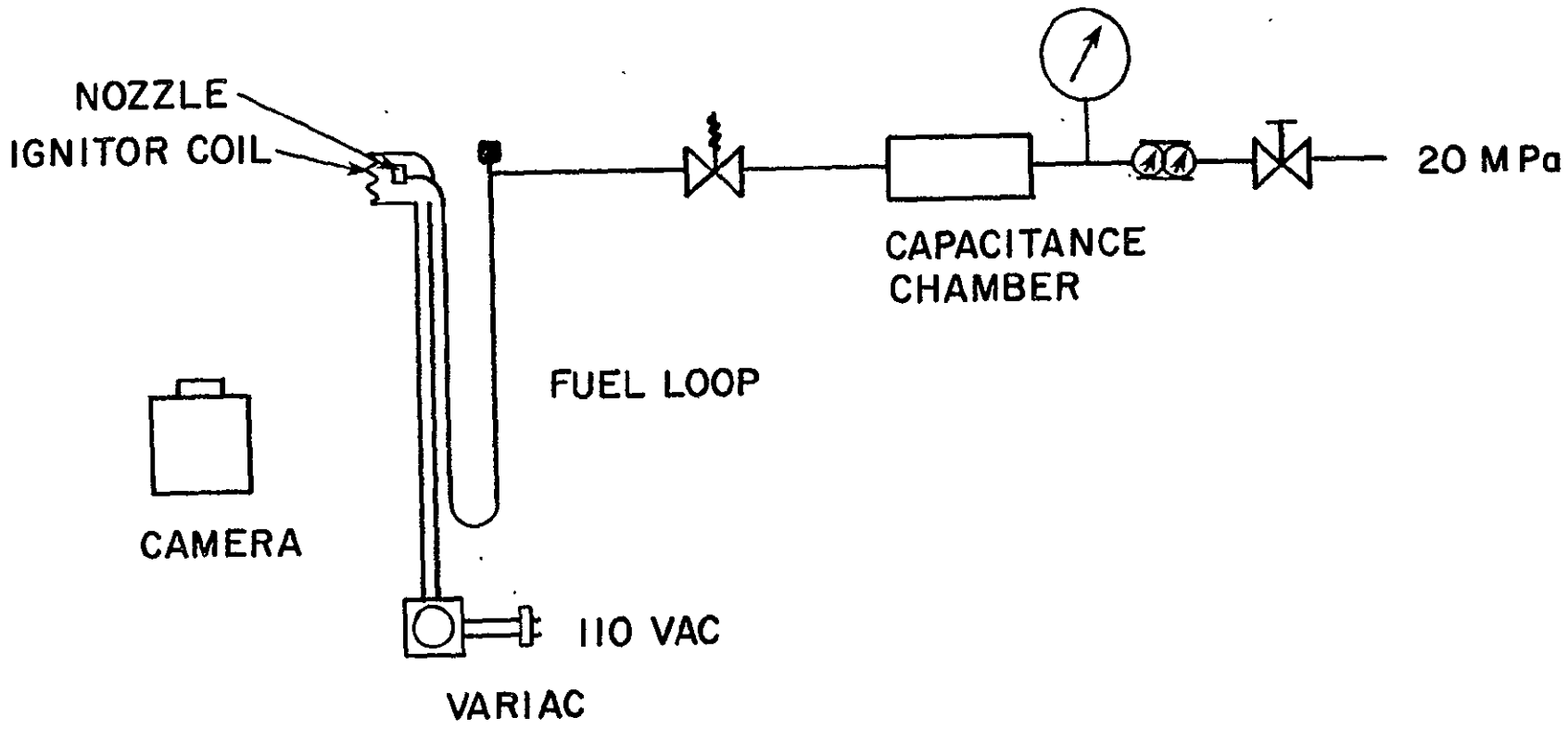

Figure 7 Sketch of the Low Pressure Apparatus

had to be moved in order to obtain a complete picture of the process. For each location several tests were recorded in order to obtain an average value for the boundaries at a particular test condition.

At each test pressure, shadowgraph photography was used to determine the spray boundaries; dark field photographs were employed for the flame boundaries. A typical example of a turbulent spray flame is shown in Figure 8. The fluctuation in the boundaries due to the unmixedness of the spray process are very apparent. The irregularities in the boundaries demonstrate the need for a statistical approach in determining the boundaries.

The photographs were analyzed frame-by-frame using a microfilm viewer. The position of the boundaries was determined by measuring the distances on the viewer and then scaling the measurement back to true size based on the nozzle width. Radial positions were measured at several axial locations along the spray and the spray penetration distances were also recorded. These distances were then averaged in order to determine the mean positions.

Each test required the pressure vessel to be disassembled. During this period the chamber was purged of any combustion products from previous tests and the windows cleaned of any soot and condensed water droplets. Fuel could then be loaded into the fuel loop and the chamber reassambled for the next test.

The chamber was then pressurized to the given test condition. The pressurization process occurred very slowly in order to permit the gas and the fuel slug to come into thermal equilibrium with the chamber. Once the given test condition was reached, the variable

Figure 8 Photograph of a Pentane Spray Flame at Atmospheric Pressure

transformer was adjusted until the ignitor coil just began to glow red and the cycling timer actuated.

CHAPTER III

THEORETICAL CONSIDERATIONS

3.1 Introduction

The theoretical objective of this investigation was to examine the ability of an integral model, which assumes a locally homogeneous flow, to predict spray boundaries and flame shapes at high pressures. Major emphasis was placed upon determining the effectiveness of the model as the ambient pressure increased. The present theory is similar in many respects to that of Reference (16) for the combustion of a submerged oxidizer jet in a liquid metal. The major difference is that the present investigation must consider the evaporation of the liquid fuel droplets and the gas in the continuous phase.

The general approach of the analysis will involve the assumption of similar profiles for various quantities. Integration of the conservation equations, in conjunction with an entrainment expression proposed by Morton (19), yields correlations of enthalpy decrement, concentration, and velocity throughout the spray. The analysis also provides an estimation of the pentration length and the radial boundaries of the spray as well as the flame boundaries.

The present investigation considers a reacting spray combustion process. The flow consists of a region of liquid fuel droplets surrounded by a region of fuel vapor and product gas, finally bounded by a reacting interface with a stagnant air environment. The major assumptions in the analysis are as follows:

1) The flow is considered to be a steady axisymmetric jet issuing into an infinitely large quiescent environment.
2) The flow field is considered to be at constant pressure.
3) The vapor and liquid phases are in local homogeneous equilibrium, i.e., they have the same local velocity and temperature.
4) Only turbulent transport processes are considered.
5) Radial gradient terms are much greater than axial gradient terms.
6) Magnitudes of fluctuating quantities are small compared to magnitudes of mean values.
7) The jet entrains material from the environment according to the entrainment expression developed by Morton (19).
8) Combustion occurs as a one-step chemical reaction.
9) The reaction rate is infinitely great and the reaction itself is localized in the flame zone. The effect of unmixedness is handled using the same approach as in Reference (16).
10) Buoyancy forces are neglected.
11) Flow properties are uniform across the width of the jet at the injector exit.
12) Mean profiles of axial mass flux, momentum flux and energy flux are assumed to be similar in shape at all positions in the jet.
13) The ideal gas law will be used to model the gas phase properties.

14) Constant specific heats will be employed to describe the enthalpy variations.

3.2 Prediction of the Penetration Length

Under these assumptions the integral equations of conservation of mass, momentum, energy, and species are:

$$\frac{d}{dz}\int_o^\infty \rho u r dr = -\,(r\rho v)_{r=\infty} \tag{3.1}$$

$$2\pi\int_o^\infty \rho u^2 r dr = \pi r_o^2 \rho_o u_o^2 = \dot{M}_o \tag{3.2}$$

$$2\pi\int_o^\infty \rho u \Delta h r dr = \dot{m}_o \Delta h_o \tag{3.3}$$

$$2\pi\int_o^\infty \rho u \Delta y r dr = \dot{m}_o \Delta y_o \tag{3.4}$$

where

$$\Delta h = h - h_\infty \tag{3.5}$$

and

$$\Delta y = \frac{c_{OX} y_F}{c_F y_{OX_\infty}} = \frac{y_{OX}}{y_{OX_\infty}} + 1 \tag{3.6}$$

The variable Δy defined in Equation (3.6) is a Shvab-Zeldovich variable which results from eliminating the reaction rate terms between the equation of conservation of species for the fuel and oxidizer.

The initial condition on the above set of equations is

$$2\pi\int_o^\infty \rho u r dr = \dot{m}_o \quad , \qquad z = 0 \tag{3.7}$$

The boundary conditions for a quiescent environment having a constant composition are:

$$u = \Delta h = \Delta y = 0 \ , \qquad \rho = \rho_\infty \ ; \qquad r = \infty \tag{3.8}$$

The dependent variables in Equations (3.1)-(3.4) are now normalized in terms of their centerline values at each axial station of the jet:

$$f_1(\eta) = \rho u/\rho_c u_c \tag{3.9}$$

$$f_2(\eta) = \rho u^2/\rho_c u_c^2 \tag{3.10}$$

$$f_3(\eta) = \rho u \Delta h/\rho_c u_c \Delta h_c \tag{3.11}$$

$$f_4(\eta) = \rho u \Delta y/\rho_c u_c \Delta y_c \tag{3.12}$$

where

$$\eta = r/a(z) \tag{3.13}$$

It is now assumed that the f_i are similar at all axial locations and the following integral constants are defined

$$I_i = \int_o^\infty f_i(\eta)\eta d\eta \ ; \qquad i = 1, 2, 3, 4 \tag{3.14}$$

The values of these integrals only change when the assumed profiles are changed, and they are constant for fully developed flow under the present assumptions.

The entrainment of the jet is represented by a model suggested by Morton (19), which has been found to be valid for the self-preserving region of the jet. The form of the entrainment expression is:

$$(-2\pi r\rho v)_{r=\infty} = 2\pi\rho_\infty E a u_c (\rho_c/\rho_\infty)^{1/2} \tag{3.15}$$

where E is the entrainment constant for the jet. The value of the

entrainment constant is dependent upon the assumed shape of the profiles, the characteristic radial scale factor and the normalizing values of density and velocity used in the expression.

The form of the equations may now be simplified by introducing a new radial scale suggested by Morton (19) for large density differences. The new scale length is defined by:

$$b(z) = a(z)(\rho_c/\rho_\infty)^{1/2} \tag{3.16}$$

and reduces the governing equations to a form that is similar to a constant density homogeneous jet.

Substituting Equations (3.9)-(3.16) into Equations (3.1)-(3.14) and rearranging yields the following set of equations.

$$\frac{d}{dz}(u_c b^2 I_1) = E b u_c \tag{3.17}$$

$$2\pi\rho_\infty u_c^2 b^2 I_2 = \dot{M}_o \tag{3.18}$$

$$2\pi\rho_\infty u_c b^2 \Delta h_c I_3 = \dot{m}_o h_o \tag{3.19}$$

$$2\pi\rho_\infty u_c b^2 \Delta y_c I_4 = \dot{m}_o y_o \tag{3.20}$$

Transforming the initial condition yields

$$2\pi\rho_\infty u_c b^2 I_1 = \dot{m}_o \; ; \qquad z = 0 \tag{3.21}$$

The solution of Equations (3.17)-(3.20) yields

$$\frac{(\pi\rho_\infty \dot{M}_o)^{1/2} b}{\dot{m}_o} = \frac{1}{I_1}\left[\frac{I_2}{2}\right]^{1/2} \Phi \tag{3.22}$$

$$\frac{\dot{M}_o}{\dot{m}_o u_c} = \frac{I_2}{I_1}\Phi \tag{3.23}$$

$$\frac{\Delta h_o}{\Delta h_c} = \frac{I_3}{I_1} \Phi \tag{3.24}$$

$$\frac{\Delta y_o}{\Delta y_c} = \frac{I_4}{I_1} \Phi \tag{3.25}$$

$$\frac{2\pi I_1 \rho_\infty u_c b^2}{\dot{m}_o} = \Phi \tag{3.26}$$

where

$$\Phi = 1 + E\left[\frac{2}{I_2}\right]^{1/2} \frac{(\pi \rho_\infty \dot{M}_o)^{1/2} z}{\dot{m}_o} \tag{3.27}$$

In order to apply these results to estimation of flame penetration length, the flame position must be specified. In the case of homogeneous laminar diffusion flames, the flame zone is very thin and it is reasonable to assume that the concentrations of fuel and oxidizer are zero at the flame. This provides a criteria $\Delta y=1$ for locating the position of the flame.

For turbulent flow, the flame zone is relatively thick and profiles of mean fuel and oxidizer concentrations overlap to a considerable extent (11, 17). Therefore, the outer limit of the combustion zone, corresponding to the point of disappearance of the injected material, occurs at values of Δy that are less than unity. In order to allow for this effect, it is assumed that the injected material is absent in the region defined by $\Delta y \leq \varepsilon_r$, where ε_r is an empirical parameter. With this specification the maximum length of the combustion process, L_r, is determined by the criteria

$$\Delta y_c = \varepsilon_r \; ; \qquad z = L_r \tag{3.28}$$

Applying the criteria of Equation (3.28) to Equations (3.25) and (3.26) yields the following expression for the penetration length

$$\frac{L_r}{d_o} = \left[\frac{I_1}{\varepsilon_r E I_4}\right]\left[\frac{I_2}{2}\right]^{1/2}\left[\frac{\dot{m}_o}{(\pi\rho_\infty \dot{M}_o)^{1/2}\, d_o B_r}\right] \tag{3.29}$$

where

$$B_r = \left[\Delta y_o - \left[\frac{I_4}{I_1}\right]\varepsilon_r\right]^{-1} \tag{3.30}$$

A penetration length correlation for an evaporating jet can also be obtained from Equations (3.24) and (3.26). For an evaporating jet, the criteria for the disappearance of liquid is that the local enthalpy must be greater than the saturated vapor enthalpy at the chamber pressure. Allowing for the unmixedness of turbulent flow, as before, provides the following specification for the maximum lengthwise position of the liquid.

$$\Delta h_c = \varepsilon_g (h_g - h_\infty) = \varepsilon_g \Delta h_g \tag{3.31}$$

where h_g is the saturated vapor enthalpy and ε_g is an empirical parameter less than unity.

The correlation for liquid penetration length becomes

$$\frac{L_g}{d_o} = \left[\frac{I_1}{\varepsilon_g E I_3}\right]\left[\frac{I_2}{2}\right]^{1/2}\frac{\dot{m}_o}{(\pi\rho_\infty \dot{M}_o)^{1/2}\, d_o B_g} \tag{3.32}$$

where

$$B_g = \left[\frac{\Delta h_o}{\Delta h_g} - \left[\frac{I_3}{I_1}\right]\varepsilon_g\right]^{-1} \tag{3.33}$$

The combined correlation of spray and flame lengths from Reference (16) is shown in Figure 3.

A correlation of velocity along the centerline of the jet may also be obtained for large z/d_o, by considering Equations (3.23) and (3.27). The centerline velocity may be represented by

$$\frac{\dot{M}_o}{\dot{m}_o u_c} = \frac{I_2}{I_1}\left[\frac{2}{I_2}\right]^{1/2} \cdot \frac{E(\pi\rho_\infty \dot{M}_o)^{1/2} z}{\dot{m}_o} \tag{3.34}$$

This correlation is shown in Figure 9 from Reference (16).

Avery and Faeth (16) demonstrated that enthalpy decrement ratios and nozzle fluid concentrations varied in the same manner, these results are illustrated in Figure 10. This suggests that I_3 and I_4 are equal. Equations (3.24) and (3.25) may be combined into the form

$$\frac{\Delta h_c}{\Delta h_o} = \frac{\Delta y_c}{\Delta y_o} \tag{3.35}$$

The enthalpy decrement ratio may be calculated from the expression

$$\frac{\Delta h_c}{\Delta h_o} = \frac{\sum_{i=1}^{n} y_i (h_f + c_p \Delta T_c)\big|_i - \sum_{i=1}^{m} y_i (h_f + c_p \Delta T_\infty)}{\sum_{i=1}^{R} y_i (h_f + c_p \Delta T_o)\big|_i - \sum_{i=1}^{m} y_i (h_f + c_p \Delta T_\infty)} \tag{3.36}$$

where

$$\Delta T = T - T_\infty \tag{3.37}$$

The fluid concentrations may be derived from the Shvab-Zeldovich variables.

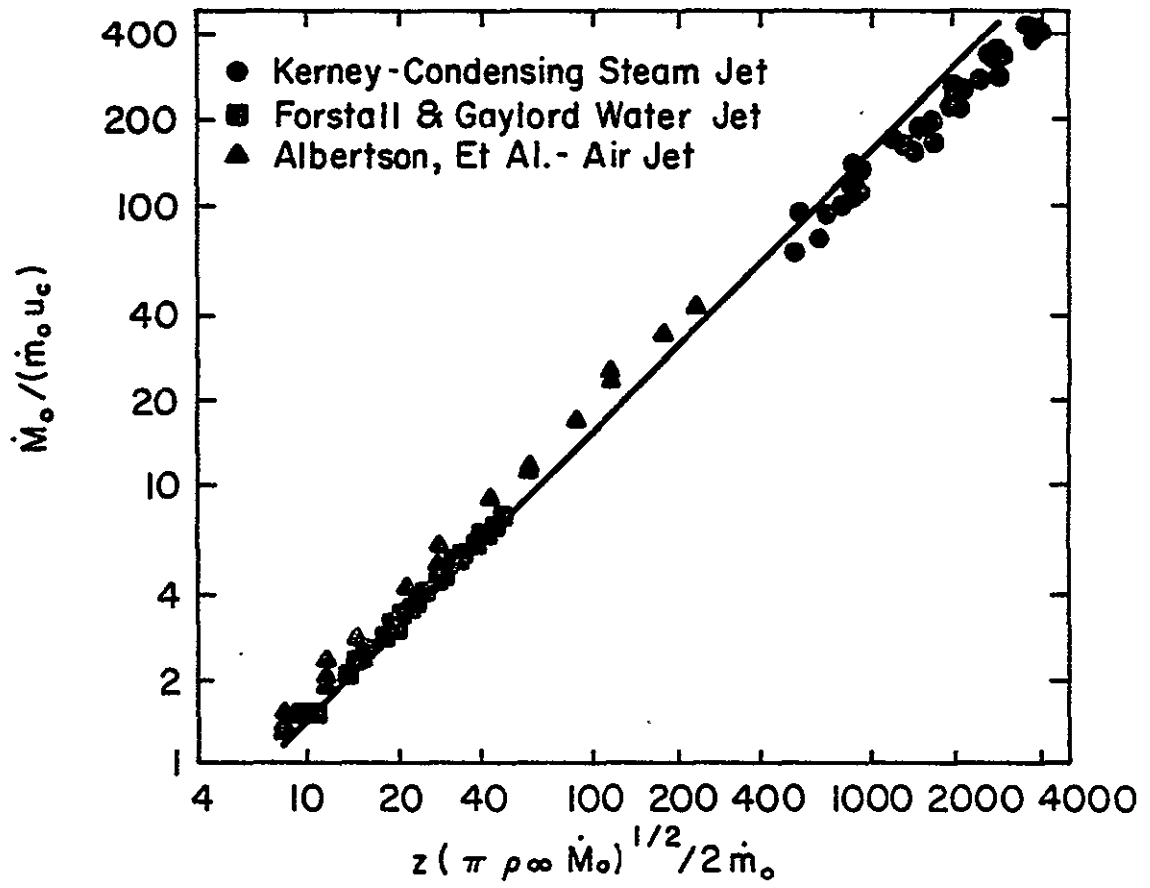

Figure 9 Correlation of Centerline Velocity, Reference (16)

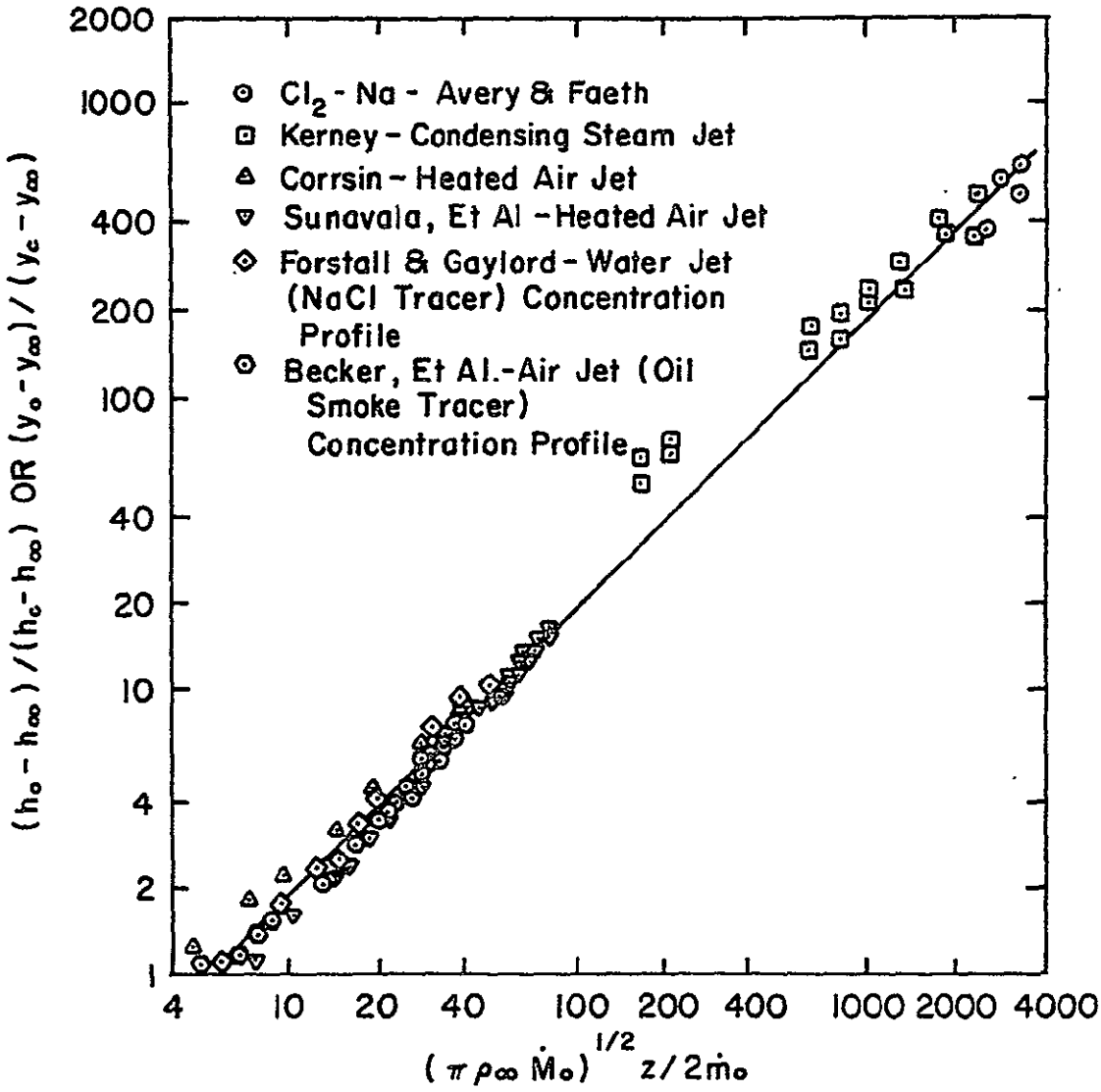

Figure 10 Correlation of Centerline Scalar Quantities, Reference (16)

$$y_F = \left[\left(\frac{\Delta y}{\Delta y_o}\right) (\Delta y_o - 1.0)\right] (c_F y_{OX,\infty}/c_{OX}) \tag{3.38}$$

$$y_W = \left[\frac{\Delta y}{\Delta y_o} - 1.0\right] (c_W y_{OX,\infty}/c_{OX}) \tag{3.39}$$

$$y_{CO_2} = \left[\frac{\Delta y}{\Delta y_o} - 1.0\right] (c_{CO_2} y_{OX,\infty}/c_{OX}) \tag{3.40}$$

$$y_{N_2} = \left[1.0 - \frac{\Delta y}{\Delta y_o}\right] y_{N_2,\infty} \tag{3.41}$$

The temperature at the penetration length of the spray boundaries may be calculated using Equations (3.36)-(3.41). Concentrations of the species are calculated at selected values of $\Delta y/\Delta y_o$ and used to calculate $\Delta h_c/\Delta h_o$ until the selected value of $\Delta y/\Delta y_o$ equals the calculated value of $\Delta h/\Delta h_o$ as required by Equation (3.35).

The penetration length for the fuel spray boundaries is calculated using the above procedure. The driving potential for evaporation B_g, in Equation (3.33) may be calculated using the computed value of $\Delta h/\Delta h_o$. The fuel spray penetration length in Equation (3.32) can then be determined.

Analysis of the temperatures in the fuel spray region indicated that condensed water vapor is present in some circumstances. The calculation procedure can also be used to determine the spray penetration length of the condensed water vapor using Equations (3.32) and (3.33).

The presence of both liquid and gaseous fuel must be considered in the spray region. The vapor pressure of the fuel was calculated from a relationship of the form

$$\log_{10} P = A - \frac{B}{(C+T)} \tag{3.42}$$

The mass fraction of fuel may be computed from the following relation

$$y_{F,G} = \frac{P_F W_{F\,i} \sum_{i=1}^{h} y_i}{\sum_{i=1}^{h} P_i W_i} \tag{3.43}$$

The mass fraction of the liquid fuel can also be determined

$$y_{F,\,L} = y_F - y_{F,G} \tag{3.44}$$

The enthalpy decrement in Equation (3.33) can be calculated treating each phase of the fuel as a separate component.

3.3 Prediction of Radial Boundaries Accounting for Variable Density

The position of the radial boundaries may be predicted by extending the analysis derived for the penetration length. Equations (3.25) and (3.27) are combined to predict the axial position for a given concentration decrement into the form

$$\frac{z}{d_o} = \frac{\left[\frac{I_1\,\Delta y_o}{I_4\,\Delta y_o} - 1\right]}{\left[2\,E\left[\frac{2}{I_2}\right]^{1/2}\left[\frac{\rho_\infty}{\rho_j}\right]^{1/2}\right]} \tag{3.45}$$

The characteristic length scale may be computed by combining Equations (3.16) and (3.22) into the following relationship.

$$a = \frac{\Phi(I_2/2)^{1/2}}{2\,I_1}\, d_o\left[\frac{\rho}{\rho_\infty}\right]^{1/2} \tag{3.46}$$

where

$$\Phi = 1 + 2\,E\left[\frac{2}{I_2}\right]^{1/2}\left[\frac{\rho_\infty}{\rho_o}\right]^{1/2}\frac{z}{d_o} \tag{3.47}$$

Tross (8) demonstrated that the normalized functions described by Equations (3.9)-(3.12) may be written as

$$f_i(\eta) = \text{Exp}\left[- K_i \eta^2\right]; \; i = 1, 2, 3, 4 \tag{3.48}$$

Substitution of Equation (3.48) into Equation (3.14) yields

$$I_i = \int_o^\infty \text{Exp}\left[- K_i \eta^2\right] \eta d\eta \; ; \quad i = 1, 2, 3, 4 \tag{3.49}$$

Integration of the above expression yields

$$I_i = \frac{1}{2K_i} \; ; \quad i = 1, 2, 3, 4 \tag{3.50}$$

The nondimensional functions represented by Equation (3.48) can now be expressed by the following relationship

$$f_i(\eta) = \text{Exp} -\left[\frac{\eta^2}{2I_1}\right] \tag{3.51}$$

The dimensionless radial distance η can be represented as a function of the concentration decrement by combining Equations (3.9), (3.12) and (3.51)

$$\eta = \left[\frac{-2 \; \ell n\left[\frac{\Delta y}{\Delta y_c}\right]}{\left[\frac{1}{I_4} - \frac{1}{I_1}\right]}\right]^{1/2} \tag{3.52}$$

By combining Equations (3.13), (3.16), (3.46) and (3.52) the radial distance may be expressed as

$$\frac{r}{r_o} = \left[\frac{-2 \; \ell n\left[\frac{\Delta y}{\Delta y_c}\right]}{\left[\frac{1}{I_4} - \frac{1}{I_1}\right]}\right]^{1/2} \left[\frac{\rho_o}{\rho_c}\right]^{1/2} \left[\frac{\Phi}{I_1}\right]\left[\frac{I_2}{2}\right]^{1/2} \tag{3.53}$$

3.4 Prediction of Incompressible Radial Boundaries

The outer location of the liquid fuel droplets is bounded by the spray boundary while the outermost location of fuel vapor is

indicated by the flame boundary. It is necessary to determine a relationship between the radial spread of the jet and axial position. The spreading rate of the jet will be taken to be the same as an incompressible jet.

Comparison of the normalized radial boundaries measured by Tross (8), Hetšroni and Sokolov (5) and McCreath and Chigier (13) indicate that the radial spread of the velocity in the spray is not strongly influenced by the density ratio of the spray to the ambient environment. Figure 11 compares the radial spread of steam-water jets, isothermal air jets and isothermal heterogeneous jets. These data encompass jets having density ratios greater than, equal to, and less than the ambient fluid.

The influence of chemical reaction on the radial spread was considered by Chigier and Roett (12). The effect of chemical reaction on the radial spread of homogeneous and heterogeneous jets is shown in Figure 12. The reacting and nonreacting heterogeneous sprays are seen to be very similar. The presence of chemical reaction decreases the radial velocity distribution for the homogeneous jets. Chigier and Roett (12) demonstrated that the velocity distributions may be expressed in the form

$$\frac{u}{u_c} = \mathrm{Exp}\left[\frac{-r^2}{2\ c_m{}^2 z^2}\right] \tag{3.54}$$

The spreading coefficients for the sprays described in Figures 11 and 12 are shown in Table 1. The density variation between the injected fluid and the ambient fluid range from 1/1000 for the steam-water system to 660 for the oil drop-air system. The value of the spreading

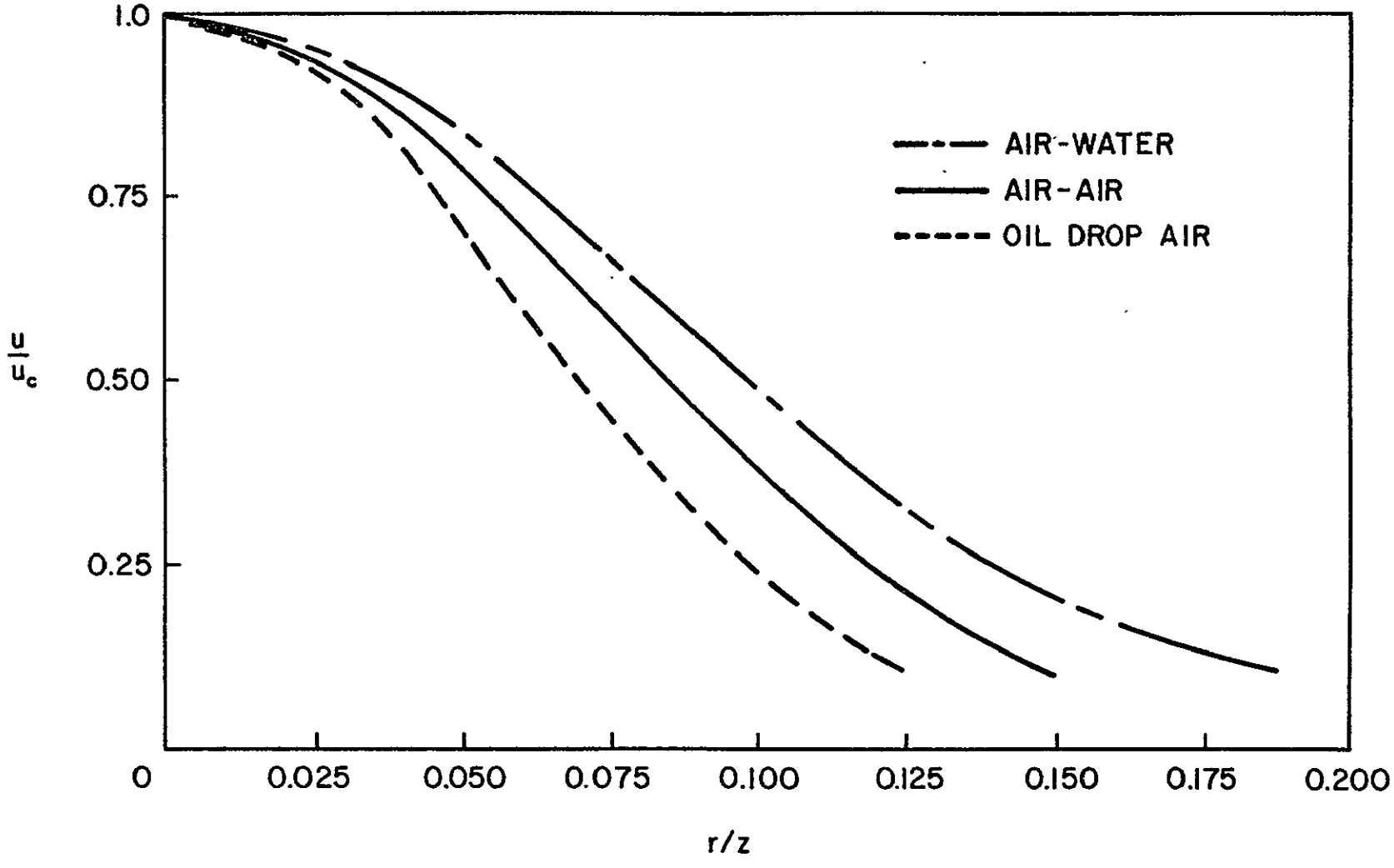

Figure 11 Spreading Characteristics of Isothermal Jets, Reference (8)

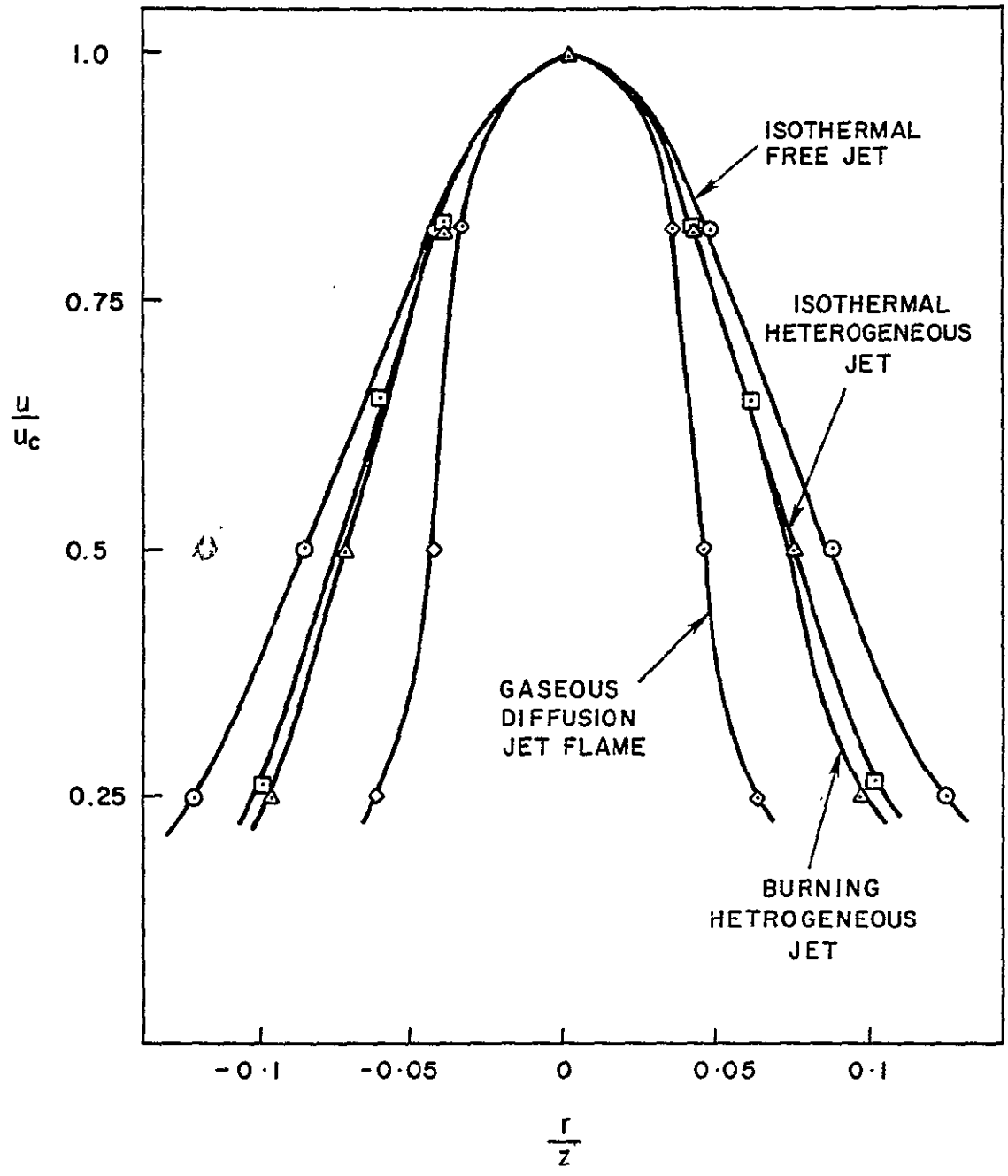

Figure 12 Spreading Characteristics of Reacting and Nonreacting Jets, Reference (12)

Table 1

Comparison of Jet Spreading Coefficients

Type of Jet	C_m
Isothermal air-air jet, Chigier and Roett (12)	.0713
Isothermal oil drop-air spray, Hetsroni and Sokolov (5)	.0645
Combusting gaseous jet, Chigier and Chervinsky (21)	.0373
Combusting spray, Chigier and Roett (12)	.0620
Air-water jet, Tross (8)	.0802

coefficient remains relatively constant for large density variations.

Hetsroni and Sokolov (5) suggested the following expression for the radial spread of fluid concentration of a spray

$$\frac{\Delta y/\Delta y_o}{\Delta y_c/\Delta y_o} = \text{Exp}\left[\frac{-r^2}{2\ c_m^2 z^2}\right] \tag{3.55}$$

where c_m is the spreading coefficient of the fluid concentration from the data of Hetsroni and Sokolov (5)

$$c_m = .05 \tag{3.56}$$

The value of $\Delta y/\Delta y_o$ is fixed by the value of this quantity at the penetration length position. Equation (3.55) is used to calculate the radial position of the boundaries of the flame, the liquid fuel, and the condensed water droplets.

3.5 Evaluation of Integral Constants

In order to complete the general model of the turbulent jet combustion process, the integral constants, entrainment constant, and unmixedness factor must be defined. Avery and Faeth (16) defined three constant groups from experimental data as follows

$$\frac{I_1}{I_4(2/I_2)^{1/2}\ E\ \varepsilon_r} = 35.5 \tag{3.57}$$

$$\frac{E(2/I_2)^{1/2}\ I_3}{I_1} = 0.096 \tag{3.58}$$

$$E(2/I_2)^{1/2}\ I_2/I_1 = 0.075 \tag{3.59}$$

The constant group $E(2/I_2)^{1/2} = 0.16$ may be determined from the data of Ricou and Spalding (20).

Values of the integral constants may be determined by curve fitting velocity profiles from constant density air filter systems. The plot of combined velocity profiles is shown in Figure 13. The integral constants were determined to be equal to

$$I_1 = 0.00631 \tag{3.60}$$

$$I_2 = 0.00319 \tag{3.61}$$

Table 2 summarizes the values for the thermal constants.

Table 2

Summary of Constants for the Variable Density Model

Constant	Value
I_1	0.00631
I_2	0.00319
I_3	0.00383
I_4	0.00383
E	0.00638
ε_r	0.29

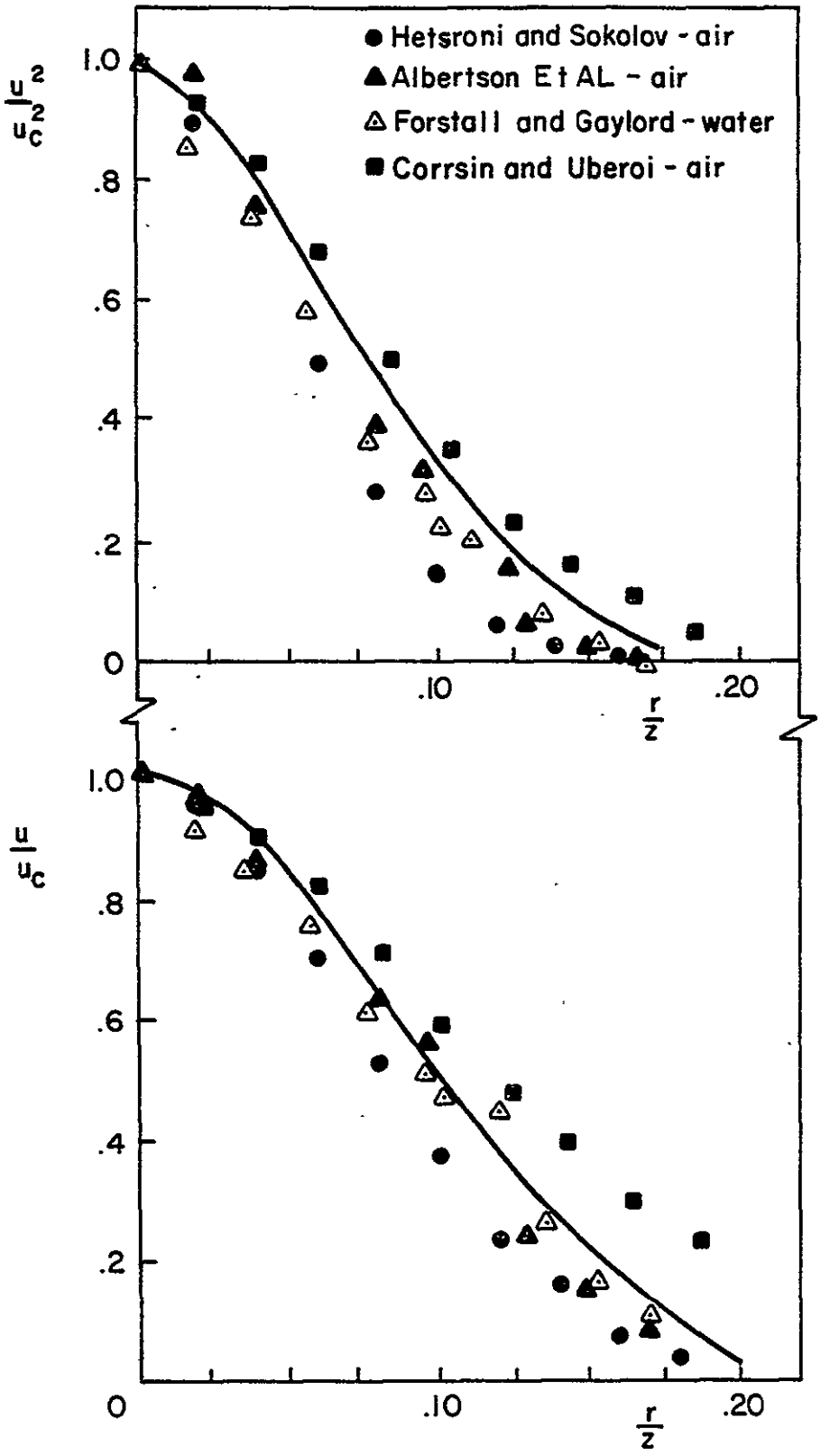

Figure 13 Correlation of Jet Velocity Spreading Characteristics

CHAPTER IV

RESULTS AND DISCUSSION

4.1 Introduction

The major objective of the present investigation was to examine the effectiveness of a locally homogeneous two-phase model for predicting the evaporation and combustion characteristics of a gas-liquid turbulent jet. It was assumed that the fuel droplets were in thermal equilibrium with the surrounding gas and moved at the local gas velocity. The liquid fuel was taken to be finely atomized at the injector exit and the flow was assumed to be fully developed immediately downstream of the injector exit. In addition the turbulent spray and flame boundaries are characterized by an irregular wavy appearance as shown in Figure 8. Estimates of the spray and flame boundaries represent the time-averaged position of the boundaries.

A variety of test conditions were examined in the present study. Table 3 lists the test conditions for the type of boundary examined. The various properties used for the test fuels are listed in Table 4.

4.2 Nonreacting Spray

Experimentally determined radial spray boundaries for nonreacting pentane and methanol jets are shown in Figures 14 and 15. The edge of the flow field is also indicated on these figures by plotting the position where $\Delta y/\Delta y_o = .01$, for both the compressible and incompressible models. The incompressible radial spread model

Table 3

Summary of Experimental Conditions

Test Conditions[a]	Methanol	Pentane
Injector Characteristics at Atmospheric Pressure		
Sauter Mean Diameter (μm)[b]	33	28
Maximum Droplet Diameter (μm)[b]	107	79
Spray Velocity of Injector Exit (m/sec)	61.1	68.5
Cold Flow Tests		
Pressure (MPa)	3, 6, 9	3, 6, 9
Length of Flow Examined $\left[\frac{z}{d_o}\right]$	90	90
Flame Boundary Tests		
Pressures (MPa)	0.1,[c] 3, 6, 9	0.1,[c] 3, 6, 9
Length of Flow Examined $\left[\frac{z}{d_o}\right]$	60	90
Spray Boundary Tests (Combustion)		
Pressures (MPa)	3, 6, 9	3, 6, 9
Length of Flow Examined $\left[\frac{z}{d_o}\right]$	Entire Boundary	Entire Boundary

a) $T_\infty \approx C$, injector pressure drop of 2.67 MPa.

b) Calculated according to Muegle (25).

c) Entire flame boundary measured.

Table 4

Summary of Physical Properties

Property	Methanol	n-Pentane	Water
ρ_o ++ (kg/m^3)	786.7	626.14	--
$h_{f\ell}$ KJ/kg	-7640	-2397.4	-15865.8
h_{fg} KJ/kg	-6276	-2029.2	-13422.9
$C_{p\ell}$ KJ/kg K	2.505	2.330	4.18
C_{pg} KJ/kg K	1.370	1.713	2.15
P_c (bar)	79.9	33.74	--
T_c (K)	512.58	469.6	--
A^+	7.97328	6.85221	6.6788
B^+	1515.14	1064.63	573.480
C^+	232.85	232.0	260.0

+T in C and P in mmHg in Equation (3.42)

++Evaluated at 1 MPa and 298 K.

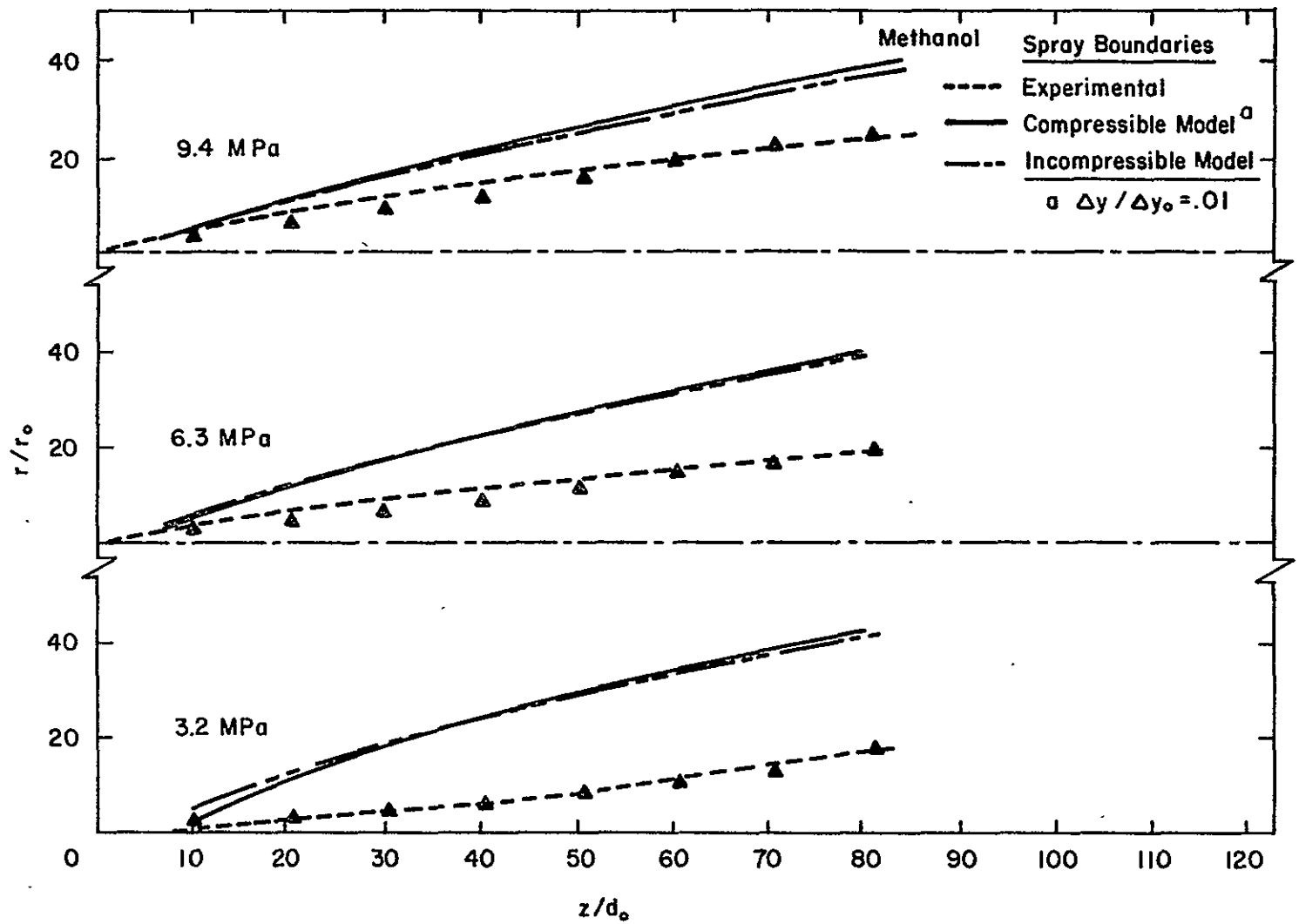

Figure 14 Nonreacting Spray Boundaries for Methanol

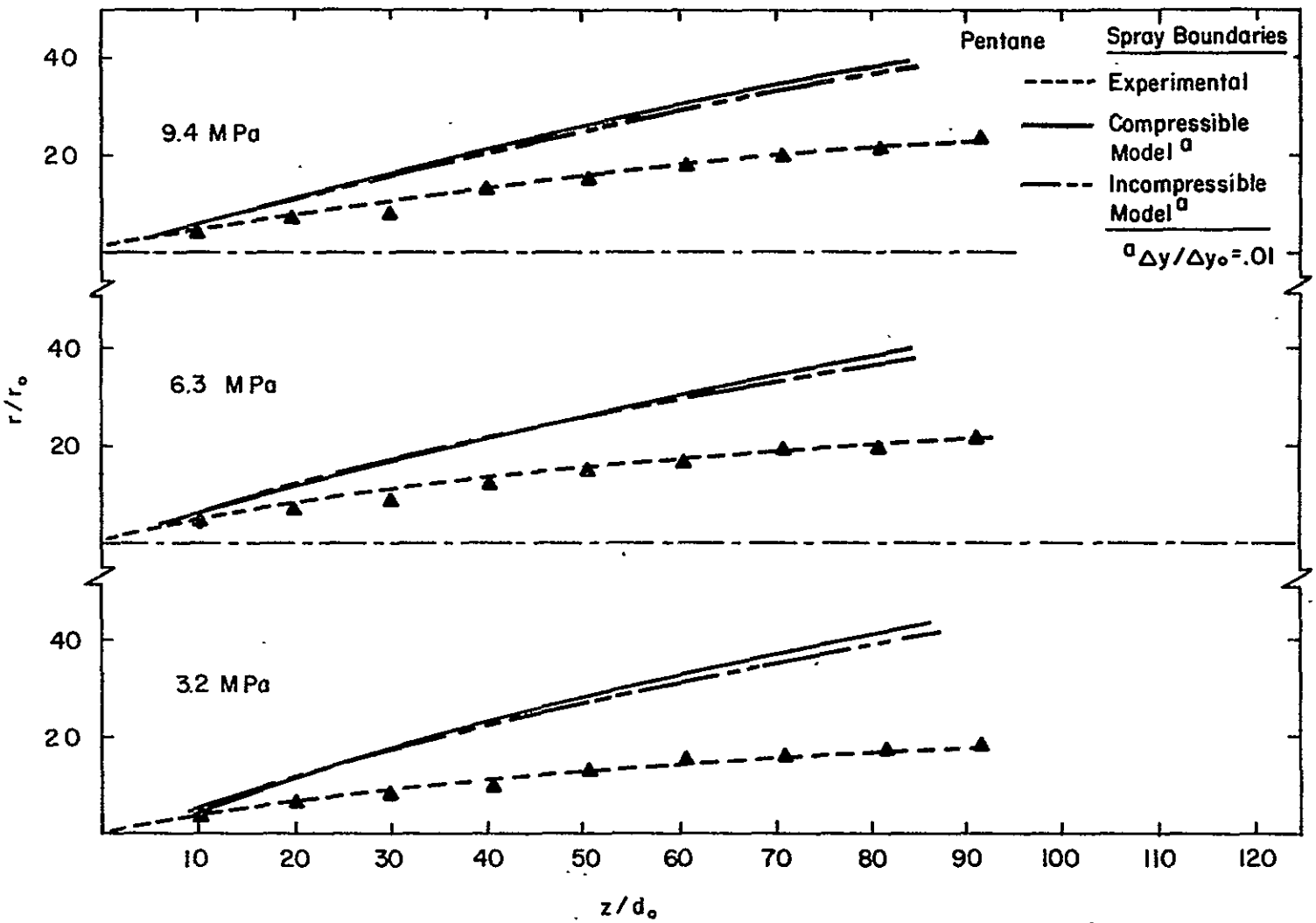

Figure 15 Nonreacting Spray Boundaries for Pentane

closely approximates the compressible radial spread model in the case of the nonreacting sprays.

In all cases the observed boundary of the spray lies well inside the conventional jet boundaries; the liquid does not appear to diffuse to the edge of the flow, as expected for locally homogeneous flow. The degree of radial liquid spread clearly increases as the pressure increases and the flow better approximates locally homogeneous flow at high pressures.

Two effects could be acting to produce the wider predicted boundaries observed in Figures 14 and 15. First of all, the outer edge of the spray is composed of fine droplets, which may not be detected with the optical system used in the current investigation. Therefore, the complete width of the spray may be wider than observed.

The second effect involves large drops in the spray following trajectories and not being diffused in the radial direction as required by a locally homogeneous model. For a given particle size, turbulent diffusion of particles is enhanced with increasing gas density. The test results, showing that the spread of the spray is greater at higher pressures, suggest that this effect is present to some degree.

In a reacting spray, the drop size decreases with distance from the injector which helps to improve the approximations of the locally homogeneous model; results of this type are discussed in the next section.

4.3 Reacting Spray Results

Predictions and measurements for methane and pentane sprays burning in air are illustrated in Figures 16 and 17, respectively. The results are given at pressures of 3, 6, and 9 MPa.

At each pressure the experimental spray length is longer for methanol than for pentane. Predicted spray lengths also follow this trend, however, the predicted lengths are only about half as long as the measurements. As in the case of the nonreactive sprays, the radial spread of the spray increases as the pressure increases.

In contrast to the nonreactive sprays, there is a substantial difference between the compressible and incompressible predictions of the radial spread of the spray. The error in spray length influences the prediction of radial boundaries, and it is difficult to decide which model is best. In general, however, it appears that the compressible model overestimates the radial spread of the spray.

The locally homogeneous models predicted that there was a region of the spray where water produced by the combustion process would condense. The predicted boundaries of this region, using the incompressible model, are also illustrated in Figures 16 and 17. In all cases, the liquid water boundary was contained within the liquid fuel boundary and the presence of water drops should not influence the experimental determination of the fuel spray boundary.

For pentane, the model indicated that drop gasification was finally completed by the fuel passing through its thermodynamic critical point at pressures of 6 and 9 MPa. All other test conditions

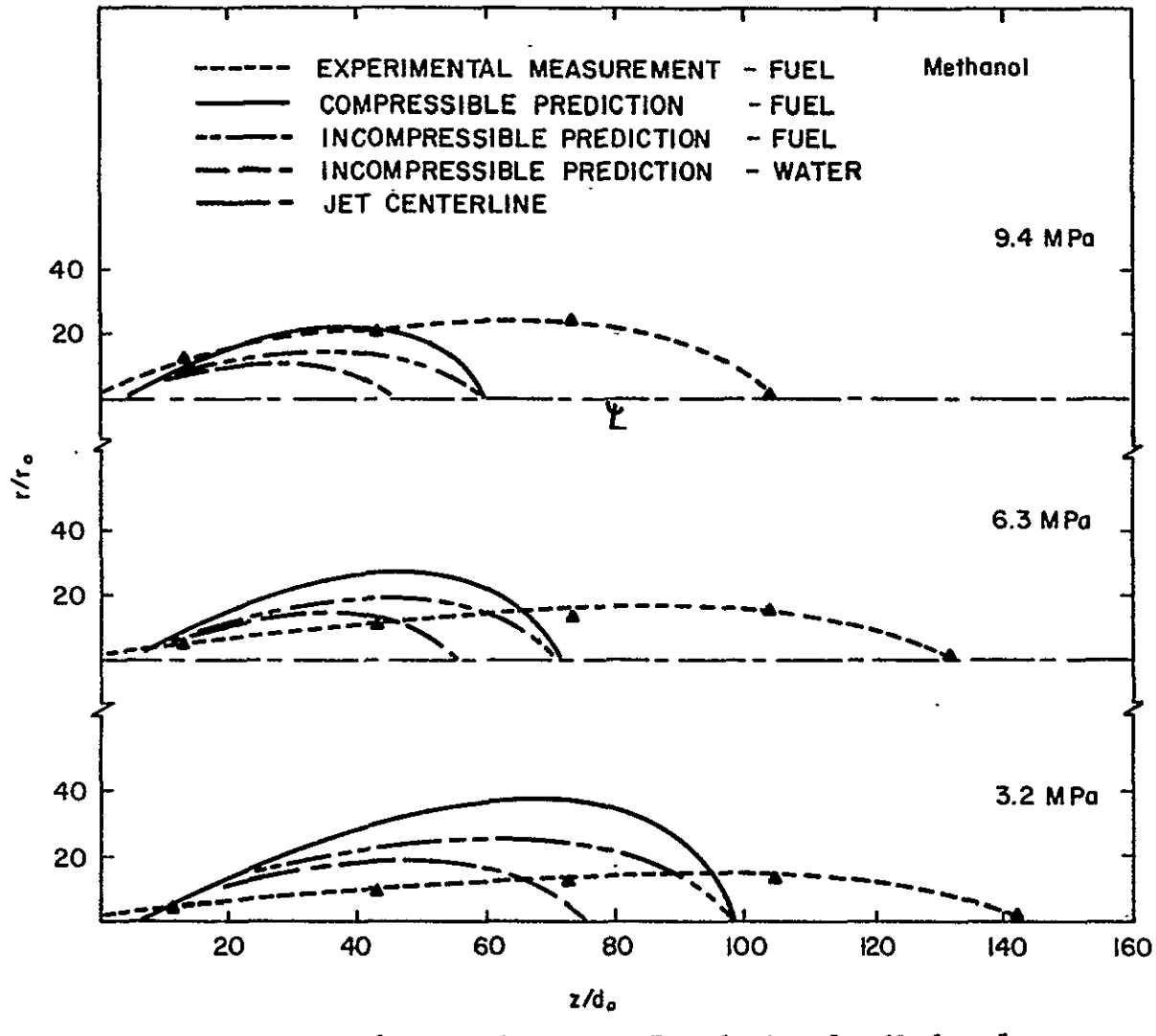

Figure 16 Reacting Spray Boundaries for Methanol

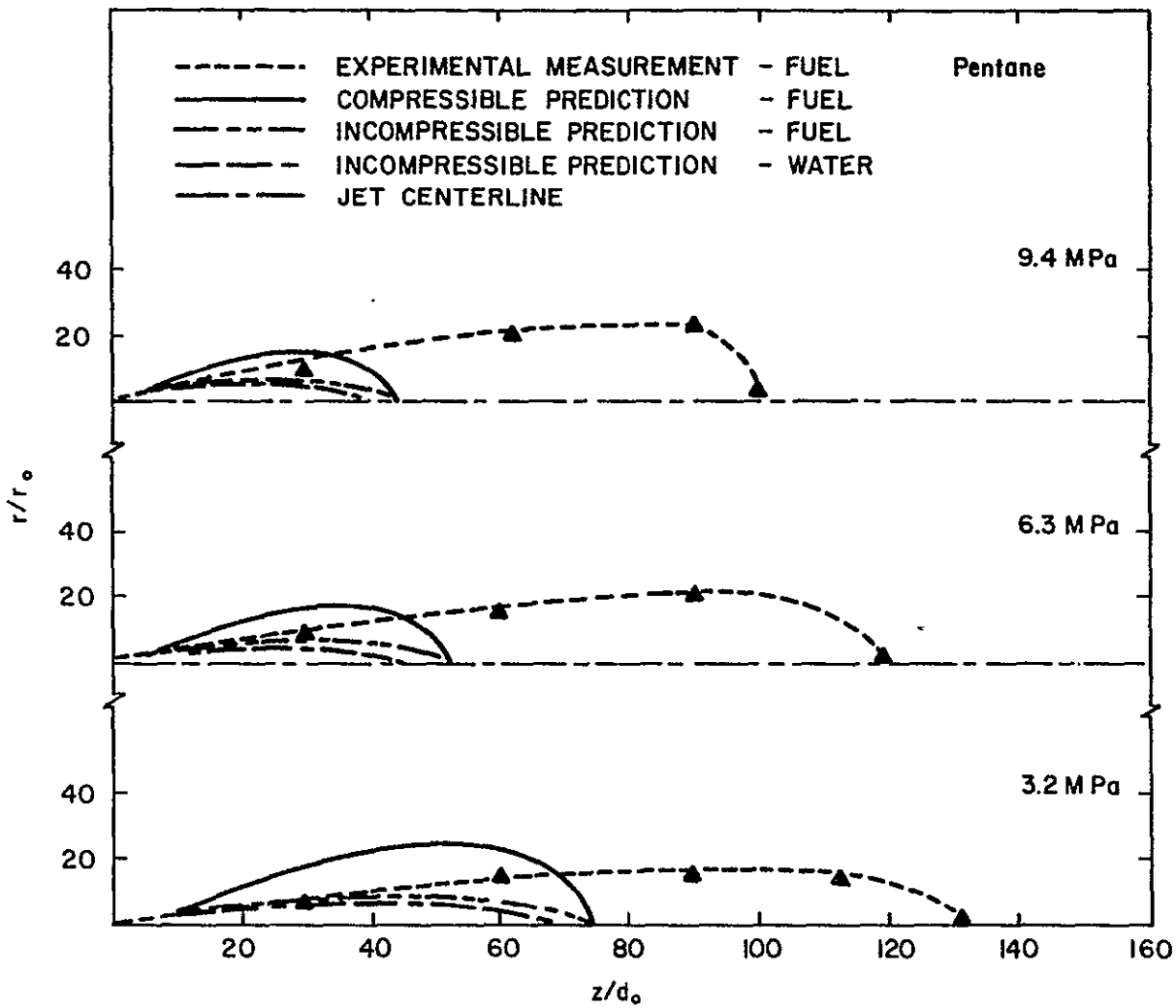

Figure 17 Reacting Spray Boundaries for Pentane

involved conventional drop evaporation at a relatively constant wet-bulb condition. Comparison between theory and experiment in Figure 17 shows no unusual change in the results for supercritical vaporization conditions. As in earlier studies of supercritical droplet combustion (1-4), the total pressure must be greater than the critical pressure for supercritical gasification to occur; although specific limits were not determined for the present test conditions. The critical pressure of methanol (7.99 MPa) is too high for supercritical evaporation to be observed during the present tests.

4.4 Flame Boundary Results

Predicted and measured flame boundaries for methanol and pentane burning in air are illustrated in Figures 18, 19 and 20. The results are given at atmospheric pressure (0.1 MPa) and pressures of 3, 6, and 9 MPa. The entire flame boundary could be obtained at atmospheric pressure. At elevated pressures, the flames were too long to obtain the entire boundary with the present apparatus, and only the initial portion of the flow is illustrated.

Flame boundaries at atmospheric pressure are illustrated in Figure 18. The locally homogeneous model gives a reasonably good prediction of the flame length for pentane, only slightly underestimating the measured length. Results are poorer for methanol, the predicted length is only about half as long as the measured value. Both models overestimate the radial position of the flame, however, the error is less for the incompressible model.

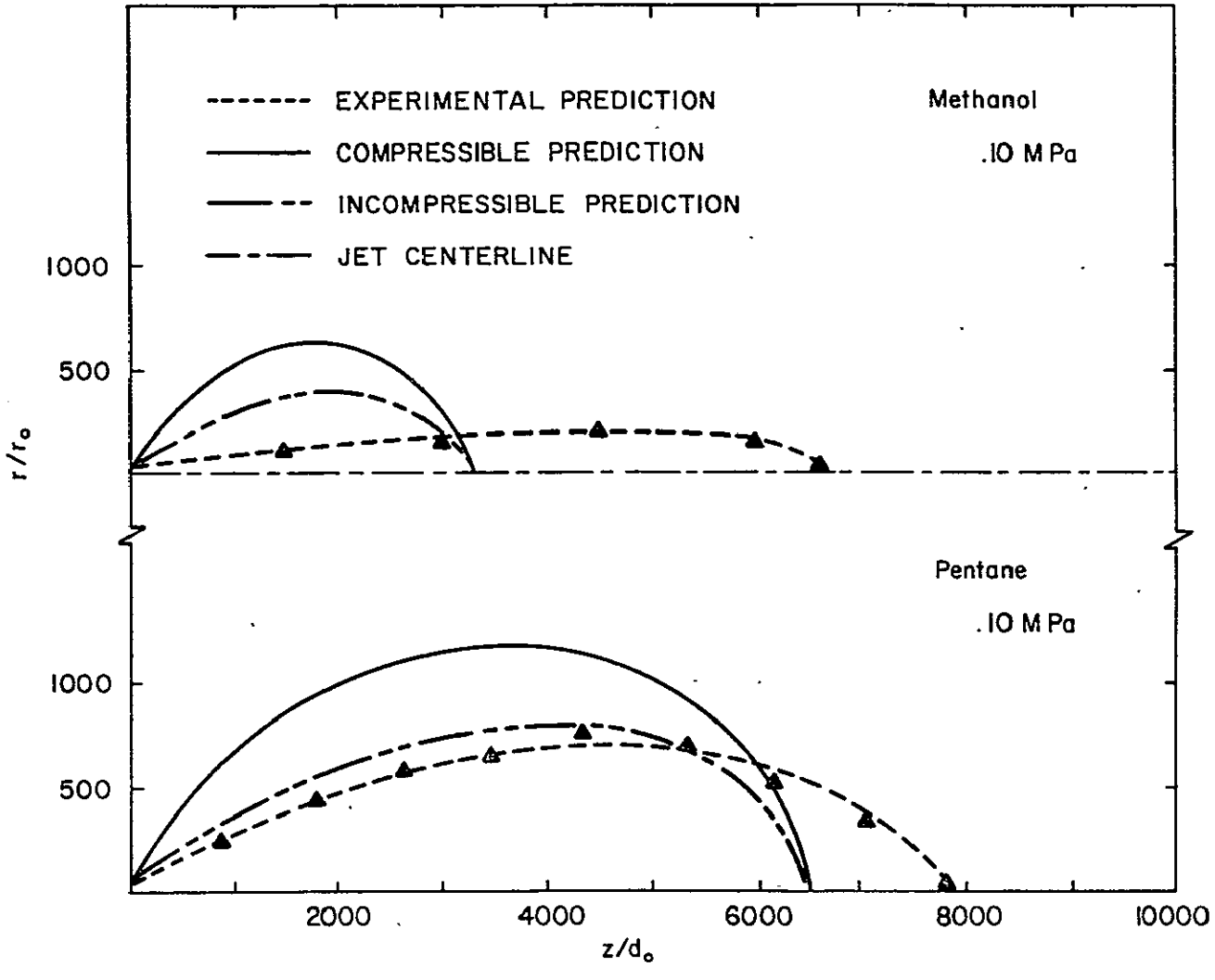

Figure 18 Flame Boundaries at Atmospheric Conditions

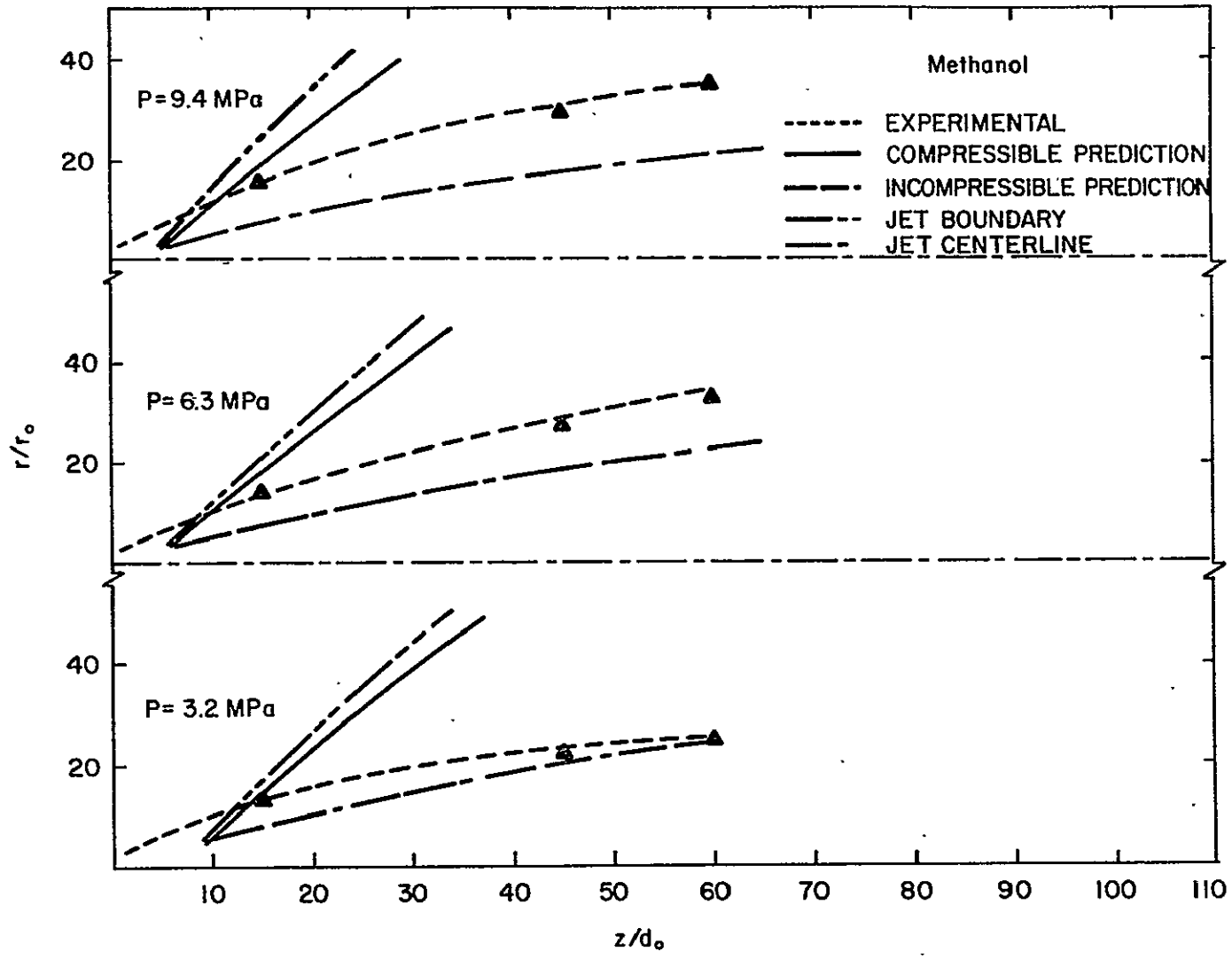

Figure 19 Flame Boundaries for Methanol

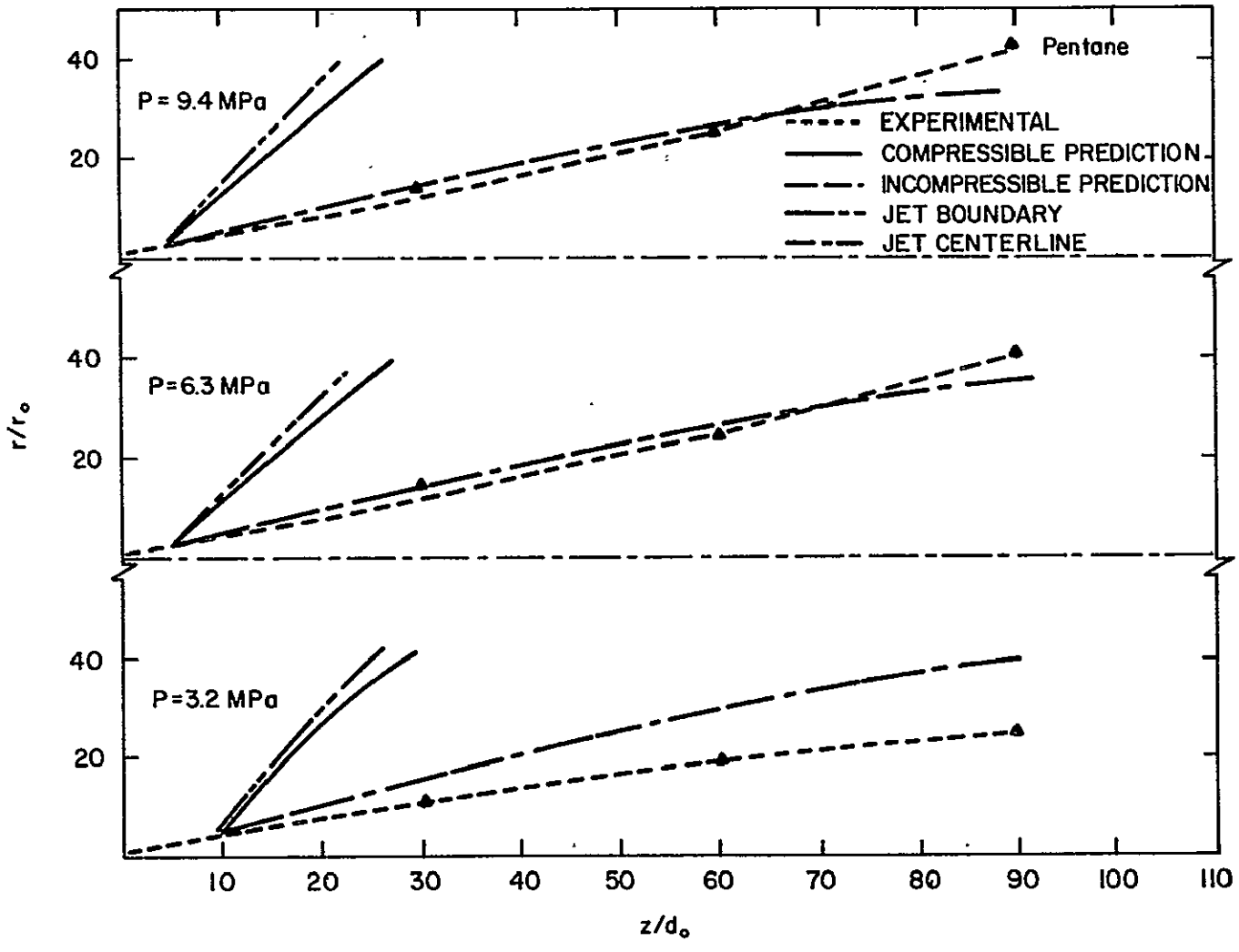

Figure 20 Flame Boundaries for Pentane.

Results at elevated pressures are illustrated in Figures 19 and 20. Similar to the spray boundaries, the measured width of the flame boundary increases as the pressure increases. The compressible model continues to overestimate the radial spread, although the incompressible model provides a reasonably good estimation of the predictions. The adequacy of the incompressible model must be treated with some reservation, however, since only the initial portions of the flame were observed at elevated pressure.

4.5 Penetration Length Results

The predictions of penetration lengths of sprays and spray flames were based on a correlation developed for gas-gas and gas-liquid systems (16). The present measurements for liquid-gas systems are compared with the original data base, and the correlation, from Avery and Faeth (16) in Figure 21. The tolerances shown on the data represent the standard deviation for the test sample at each condition. A summary of the comparison between theory and experiment is given in Table 5.

In general, the present measurements are above the correlation for both spray and flame boundaries. The model provides a qualitative estimation of the length of various phenomena, e.g., the flame length is correctly predicted to be substantially longer than the spray length, however, the theory underestimates the lengths by 30 to 50 percent.

Increasing the pressure causes a data point to shift toward the left-hand side of Figure 21. The spray length results indicate that measurements at high pressures are generally in poorer agreement with

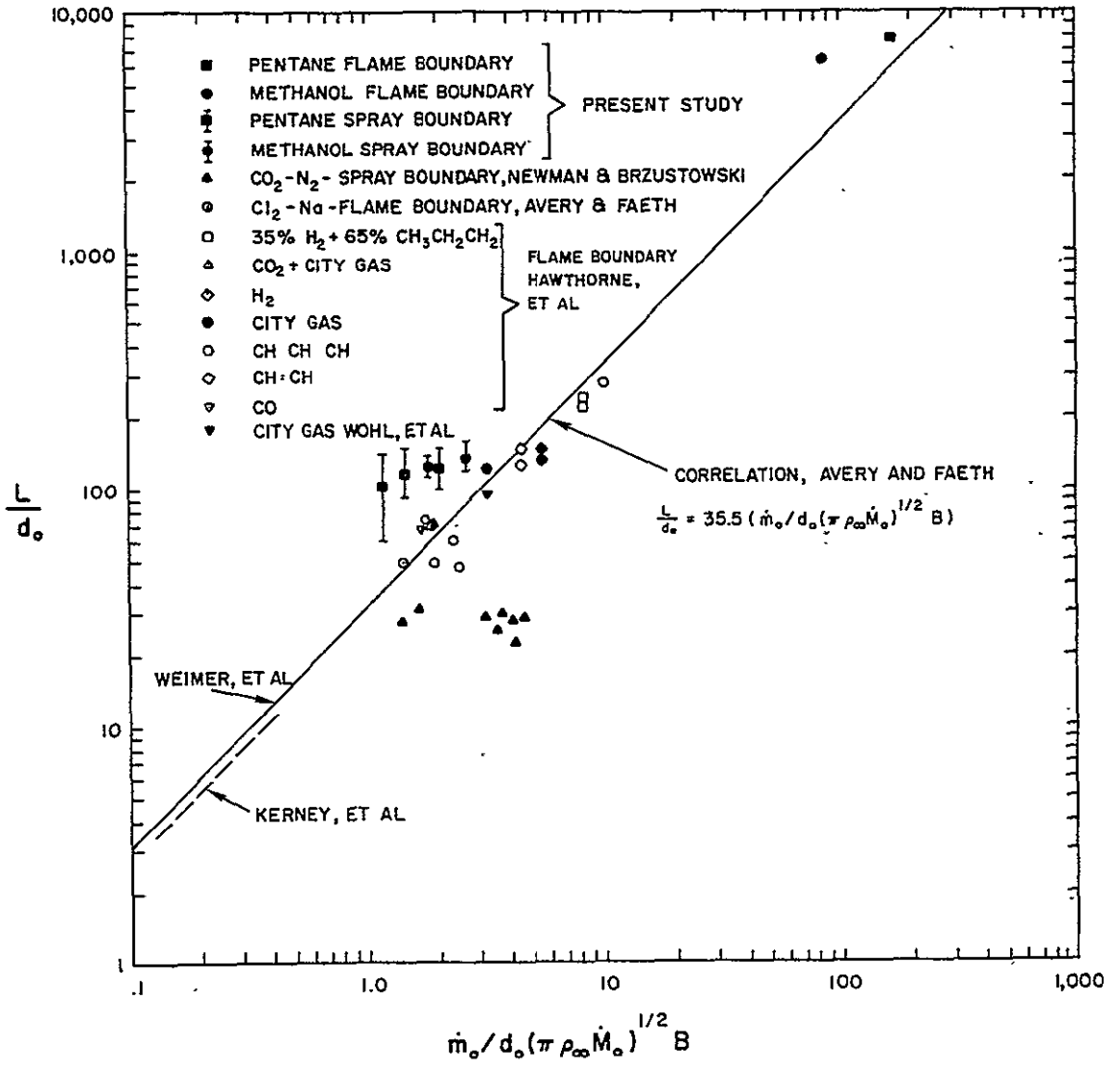

Figure 21 Correlation of Penetration Length Data

Table 5

Experimental and Predicted Penetration Lengths[a]

Pressure (MPa)	Type of Boundary	Theoretical Length L/d_o	Experimental Length L/d_o	Percent Deviation
Methanol				
0.1	Flame	3290	6640	51
3	Spray	98.9	142	31
6	Spray	70.9	132	47
9	Spray	58.5	104	44
Pentane				
0.1	Flame	6490	7850	17
3	Spray	73.8	132	44
6	Spray	52.8	119	56
9	Spray	43.1	100	57

[a]For combustion of sprays in air at 23 C.

the predictions. Behavior of this type was not expected, since the locally homogeneous model should be a better approximation of the real flow as the density ratio of the two phases approaches unity.

The spray length measurements of Newman and Brzustowski (10) for the CO_2-N_2 system are also shown in Figure 21. Their measurements fall below the present correlation although they found good agreement with their model. It is difficult to explain this behavior in view of the present results. The measurements of Reference (10) were made close to the critical point and properties are difficult to estimate in this region, which provides one explanation. The fact that Newman and Brzustowski did not have to allow for unmixedness of the turbulent flow in order to achieve good agreement between their theory and experiment also suggests that this data might be atypical. No other result illustrated in Figure 21 could be correlated in this manner. Furthermore it is unusual for the penetration length of a liquid-gas system to be overestimated by the no-slip penetration length correlation. Any slip that occurred between the droplets and the surrounding gas would have the effect of lengthening the jet.

4.6 Distribution of Centerline Velocity

The locally homogeneous integral model has been used to provide a correlation of centerline velocity using data for gas-gas and gas-liquid systems (16). The correlation has the following form

$$\frac{\dot{M}_o}{\dot{m}_o u_c} = .075\ (\pi \rho_\infty \dot{M}_o)^{1/2}\ z/\dot{m}_o \qquad (4.1)$$

The comparison between Equation (4.1) and the steam-water jets measurements of Kerney, et al., (7), and the homogeneous jet measurements of Albertson, et al., (22) and Forstall and Gaylord (23) is illustrated in Figure 22.

The correlation can be examined for liquid-gas jets using measurements provided by Newman and Brzustowski (10) for liquid carbon dioxide injected into mixtures of gaseous carbon dioxide and nitrogen at high pressures. The comparison is illustrated in Figure 22. It is evident that good agreement is obtained between the correlation developed for gas-gas and gas-liquid systems, and the measurements of Reference (10) for a spray.

4.7 Discussion of Results

Aside from the measurements of Newman and Brzustowski (10), which seem to be atypical, the model consistently underestimates the length of spray and flame boundaries. Two major factors could be responsible for this behavior: (1) inadequacies in the basic turbulent jet model, and (2) failure of the locally homogeneous model for the present two-phase flow.

The advantage of the present turbulent jet model is that it provides simple analytical expressions for mean quantities in a variable density jet. While the model has been developed using a large data base for jets, it is not very sophisticated by present day standards. In particular, the development region near the injector is not treated explicitly, and the model is only adequate at large z/d_o values. The effect of turbulent unmixedness, when treating a quantity such as a spray or flame length, is handled using a fixed value of ε;

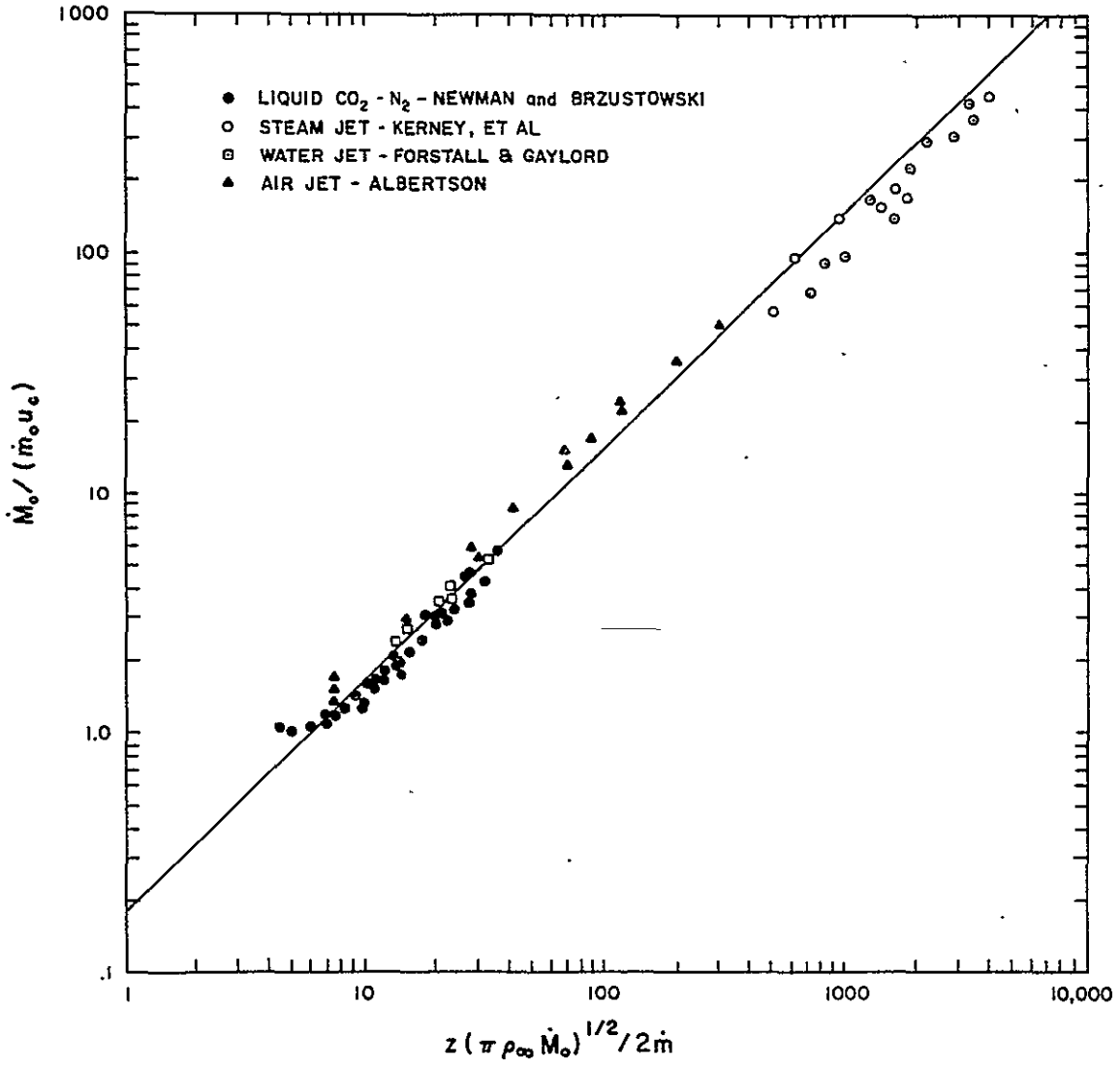

Figure 22 Correlation of Centerline Velocity Distribution for the CO_2-N_2 System

it is unlikely that a fixed value of ϵ is adequate for all circumstances.

The potential effect of the oversimplifications of the turbulent model could be evaluated using a more sophisticated calculation. Khalil and Whitelaw (15) have recently reported results of this type. Their experiment involved combustion of a kerosene spray produced by a swirl atomized injector. Two injector conditions were examined, having cold flow Sauter mean diameters of 45 and 100 μm, respectively. The injector was located at the axis of a swirling air flow. A locally homogeneous two-phase model was employed to analyze measurements of mean velocity and temperatures within the flame. A k-ϵ turbulence model was employed in the flow calculations with a clipped Gaussian probability density distribution used to represent unmixedness in the reaction rate expression.

Unfortunately, the base flow of Reference 15 is rather complex, which complicates the interpretation of the results. It was found, however, that the locally homogeneous model overestimated the rate of development of the flame, similar to the present findings. Results were poorer for the spray having the larger Sauter mean diameter. This suggests a progressive failure of the locally homogeneous model as the drop size increases. Both the present study and Reference (15) indicate that sprays having Sauter mean diameters as small as 30-45 μm are still only marginally represented by a locally homogeneous assumption. Based on this finding, it appears that weaknesses in the present turbulent flow model are not the major source of the discrepancies between measurements and predictions.

There are two aspects of the failure of a locally homogeneous model of a two-phase flow: (1) kinematic failure due to slip, and (2) failure of the assumption of thermodynamic equilibrium. Slip limits the rate at which the jet momentum is transferred to the gas phase, reducing the entrainment of the ambient gas from the levels obtained for gaseous injection with the same total momentum in the flow. Therefore, a greater length is required to entrain sufficient ambient material to gasify or burn the fuel, as observed in the present experiments.

Slip is particularly important for large drops, which carry a significant percentage of the momentum of the flow. Large drops also do not diffuse in a turbulent flow, which limits the radial spread of mass within a two-phase jet (26). Reduced levels of radial spread were observed in the present experiments for both combusting and noncombusting flows.

The radial diffusion of particles approaches turbulent gas diffusion rates as the density of the two phases approaches unity (26). The present measurements exhibit this tendency, with the high pressure sprays showing a greater lateral spread. However, penetration length predictions did not show a corresponding improvement. This behavior is due to the fact that penetration lengths of high pressure sprays are shorter, e.g., the theory implies that L is proportional to $p_\infty^{-1/2}$ for a given injector condition. Therefore, the bulk of the process moves nearer to the injector at high pressures, where problems with slip are still important.

The effect of the thermodynamic equilibrium assumption was not examined quantitatively during the present investigation, however,

it is clear that loss of thermal equilibrium due to the thermal inertia of the drops would tend to increase the length of spray and flame boundaries.

In order to improve the model, a complete two-phase turbulent flow analysis must be considered. This involves computing the life histories of the drops produced by the injector. The interaction of the drops and the gas phase must be considered, so that the environment of the drops can be determined. Analysis of this type have been reported by Crowe, et al., (27), and Jurewicz and Stock (28), although the results have not been confirmed by experiments. These calculations employ a $k-\varepsilon$ turbulence model to represent the gas phase, and allow for the distributed exchange of mass, momentum, and energy between the two phases. The most recent version allows for particle diffusion as well, although little data is available on particle diffusion rates for use in the calculations (28).

The difficulty in employing a comprehensive two-phase turbulence model for a spray is that a great deal of empirical information is required as input for the calculations. The drop size distribution of the injector, as well as the initial streamwise and radial velocity distributions for each drop size group, must be provided; this information is rarely available for practical injectors under the hot firing conditions. There are significant uncertainties in other quantities used in the model: drop transport processes, evaporation, drag, etc., in a spray environment; turbulence modeling constants; turbulence generation and dissipation by drops; turbulent drop diffusion; and proper representation of turbulent combustion processes (29).

In view of all the difficulties of a comprehensive model, the simplicity of the locally homogeneous flow assumption is very appealing. In view of potential uncertainties in input data and correlations used in a complete model, the accuracy of even the present simplified model may prove to be reasonably competitive (although the availability of a large number of parameters within a complete model provides greater scope for matching theory and experiment). Integral models, however, cannot be readily applied to the recirculating flows frequently encountered in practical combustion systems, and locally homogeneous models similar to the one used in Reference (15) are preferable in this case.

The empirical constants used in the present model were fixed by earlier gas-gas and gas-liquid measurements (16). Using these constants, the present test conditions left little room to adjust parameters and improve the predictions. It was felt that the test range of this investigation was too limited to obtain adjusted parameters for sprays. The measurements employed a narrow range of injector velocities, only two fuels, and a single injector diameter. Additional data over a broader range of variables is necessary prior to attempting a generalized correlation valid for spray.

CHAPTER V

SUMMARY AND CONCLUSIONS

5.1 Summary

This investigation considered a turbulent spray combustion process in a stagnant environment. Emphasis was placed on examining the capability of a locally-homogeneous two-phase flow model to predict the characteristics of the spray. The specific objectives of the study were as follows:

1) Measure spray and flame boundaries for combusting and noncombusting pressure atomized sprays at various ambient pressures. Methanol and n-pentane were considered at pressures in the range 0.1-9 MPa. The higher pressures in this range exceed the thermodynamic critical pressure of the fuels.

2) Available measurements were to be compared with predictions using a locally homogeneous flow model (16). The model is based on measurements in gas-gas and gas-liquid jets, but had not been examined for sprays.

The test configuration consisted of a single-hole, orifice-type injector, issuing into a stagnant environment of pure air. No swirl was applied to the liquid flow. The sprays had a Sauter mean diameter of 28-33 μm, under cold flow conditions, at atmospheric pressure.

The major results of the investigation may be summarized as follows:

1) The length of the spray boundaries decreased and the radial spread increased with increasing ambient pressure.

2) At comparable conditions, the spray length is shorter for pentane than for methanol. Flame lengths, however, show the opposite trend and methanol has the longer flame.

3) The theoretical model, based on the locally homogeneous flow approximation, correctly predicts the trends cited in Items 1) and 2). The specific correlations are given by Equations (3.29) and (3.32). The correlations consistently underestimate the measured lengths, with errors on the order of 30-50 percent. Although the present turbulence model is relatively crude, similar behavior has been reported for a k-ε turbulence model of a spray, using the locally homogeneous flow approximation (15).

4) The best prediction of radial boundaries was obtained using radial length scales for incompressible flow. This agrees with other measurements of variable density flows where it has been found that spread rates are similar to constant density flows (5, 13).

5) Mean velocities in a spray were predicted reasonably well with the present model for $z/d_o > 10$.

6) The accuracy of the predictions is poorer at high pressures even though the density ratio of the two phases approaches unity which should tend to improve the locally homogeneous approximation. This behavior appears to be due to the fact that the penetration length decreases as the pressure

increases, therefore, the bulk of the process approaches the injector where slip effects are still important.

7) The predictions indicate the presence of regions within a burning spray where water vapor produced in the combustion process should condense. For the conditions of the present experiments, the liquid water boundary always fell within the spray boundaries.

8) Predictions for pentane at 6 and 9 MPa indicate that the spray finally gasified by the drops passing through the thermodynamic critical point. The results do not indicate any unusual phenomena when this occurred.

5.2 Conclusions

The conclusions of the investigation are as follows:

1) The present locally homogeneous spray model is convenient to use, and requires a minimum amount of input data, but tends to overestimate the rate of development of the combustion process. Quantitative predictions could be improved by adjusting some of the empirical parameters within the model, from the values that were optimized for gas-gas and gas-liquid jets. However, the present test range was felt to be too limited to undertake an adjustment of this type. A larger data base, particularly including more fuel types, different injector velocities and different injector diameters is necessary before this step can be undertaken with some confidence.

2) The simple integral model used to represent the turbulent jet in this investigation is seriously limited in its capabilities to be extended to recirculating flows. Further work should consider more complete turbulence models, e.g., the model used by Khalil and Whitelaw (15), which are capable of this extension. A model of this type would remove some of the uncertainties in evaluating the locally homogeneous flow assumption. Efforts to date in two-phase flows have been limited, and further study is required to establish the range of validity of the locally homogeneous flow approximation for spray evaporation and combustion processes.

3) Spray combustion predictions attempted thus far have employed the locally homogeneous flow approximation. Models of this type have consistently overestimated the rate of development of the combustion process. More exact results require the development of complete two-phase flow models.

BIBLIOGRAPHY

1. Faeth, G. M., D. P. Dominicis, J. F. Tulpinsky, and D. R. Olson, "Supercritical Droplet Combustion," Twelfth Symposium (International) on Combustion, The Combustion Institute, Pittsburgh, Pennsylvania, pp. 9-18, 1969.

2. Lazar, R. S. and Faeth, G. M., "Bipropellant Droplet Combustion in the Vicinity of the Critical Point," Thirteenth Symposium (International) on Combustion, The Combustion Institute, Pittsburgh, Pennsylvania, pp. 801-812, 1971.

3. Canada, G. S. and Faeth, G. M., "Fuel Droplet Burning Rates at High Pressures," Fourteenth Symposium (International) on Combustion, The Combustion Institute, Pittsburgh, Pennsylvania, pp. 1345-1363, 1973.

4. Canada, G. S. and Faeth, G. M., "Combustion of Liquid Fuels in a Flowing Combustion Gas Environment at High Pressure," Fifteenth Symposium (International) on Combustion, The Combustion Institute, Pittsburgh, Pennsylvania, pp. 419-428, 1974.

5. Hetsroni, G. and Sokolov, M., "Distribution of Mass, Velocity, and Intensity of Turbulence in a Two-Phase Turbulent Jet," Transactions ASME, Journal of Applied Mechanics, Vol. 93,pp. 315-327, 1971.

6. Weimer, J. C., Faeth, G. M., and Olson, D. R., "Penetration of Vapor Jets Submerged in Subcooled Liquids," Journal-A.I.Ch.E. Vol. 19, No. 3, pp. 552-558, 1973.

7. Kerney, P. J., Faeth, and Olson, D. R., "Penetration Characteristics of a Submerged Steam Jet," Journal-A.I.Ch.E., Vol. 18, pp. 548-553, 1972.

8. Tross, S. R., "Characteristics of a Submerged Two-Phase Turbulent Free Jet," M.S. Thesis, The Pennsylvania State University, University Park, Pennsylvania, 1974.

9. Wakuri, Y., Fuji, M., Amitani, T. and Tsuneya, R., "Studies on the Penetration of a Fuel Spray in a Diesel Engine," Bulletin of the Japanese Society of Mechanical Engineers, Vol. 3., p. 123, 1960.

10. Newman, J. A. and Brzustowski, T. A., "Behavior of a Liquid Jet Near the Thermodynamic Critical Region," A.I.A.A. Journal, Vol. 9, No. 8, pp. 1590-1602, August, 1971.

11. Thring, M. W. and Newby, M. P., "Combustion Length of Enclosed Turbulent Jet Flames," Fourth Symposium (International) on Combustion, The Combustion Institute, Pittsburgh, Pennsylvania, pp. 789-796, 1953.

12. Chigier, N. A. and Roett, M. F., "Twin-Fluid Atomizer Spray Combustion," ASME Winter Annual Meeting, New York, Paper No. 72-WA/HT-25, 1972.

13. McCreath, C. G. and Chigier, N. A., "Liquid Spray Burning in the Wake of a Stabilizer Disc," Fourteenth Symposium (International) on Combustion, The Combustion Institute, Pittsburgh, Pennsylvania, pp. 1355-1363, 1973.

14. Onuma, Y. and Ogasawara, M., "Studies on the Structure of a Spray Combustion Flame," Fifteenth Symposium (International) on Combustion, The Combustion Institute, Pittsburgh, Pennsylvania, pp. 453-465, 1975.

15. Khalil, E. E. and Whitelaw, J. H., "Aerodynamic and Thermodynamic Characteristics of Kerosene-Spray Flames," Sixteenth Symposium (International) on Combustion, The Combustion Institute, Pittsburgh, Pennsylvania, in press.

16. Avery, J. A and Faeth, G. M., "Combustion of a Submerged Gaseous Oxidizer Jet in a Liquid Metal," Fifteenth Symposium (International) on Combustion, The Combustion Institute, Pittsburgh, Pennsylvania, pp. 501-512, 1974.

17. Hawthorne, W. R., Weddell, D. S., and Hottel, H. C., "Mixing and Combustion in Turbulent Gas Jets," Third Symposium on Combustion Flame and Explosion Phenomena, Williams and Wilkins Company, Baltimore, pp. 288-300, 1949.

18. Wohl, K., Gazley, C., and Kapp, N., "Diffusion Flames," Third Symposium on Combustion and Explosion Phenomena, Williams and Wilkins Company, Baltimore, pp. 288-300, 1949.

19. Morton, B. R.,"Modeling Fire Plumes," Tenth Symposium (International) on Combustion, The Combustion Institute, Pittsburgh, Pennsylvania, pp. 973-982, 1965.

20. Ricou, F. D. and Spalding, D. B., "Measurements of Entrainment by Axisymmetric Turbulent Jets," Journal of Fluid Mechanics, Vol. 11, pp. 21-32, 1961.

21. Chigier, N. A. and Chervinsky, A., "Aerodynamic Study of Turbulent Burning Free Jets with Swirl," Eleventh Symposium (International) on Combustion, The Combustion Institute, Pittsburgh, Pennsylvania, pp. 489-499, 1967.

22. Albertson, M. L., Dai, Y. B., Jensen, R. A., and Rouse, H., "Diffusion of Submerged Jets," Proceedings of ASCE, Vol. 74, pp. 1571-1596, 1948.

23. Forstall, W. and Gaylord, E. W., "Momentum and Mass Transfer in a Submerged Water Jet," Transactions, ASME, Journal of Applied Mechanics, Vol. 22, pp. 161-164, 1955.

24. Corrsin, S. and Uberoi, M. S., "Further Experiments on the Flow and Heat Transfer in a Heated Turbulent Air Jet," NACA TN-1865, April 1949.

25. Mueale, R. A., "Maximum Stable Droplets in Dispersoids," Journal - A.I.Ch.E., Vol. 6, No. 1, pp. 3-8, 1960.

26. Soo, S. L., Fluid Dynamics of Multiphase Systems, Blaisdell Publishing Company, Waltham, Massachusetts, pp. 51-60, 1967.

27. Crowe, C. T., Sharma, M. P., and Stock, D.E., "The Particle-Source-in-Cell (PSI-Cell) Model for Gas Droplet Flows," ASME Paper No. 75-WA/HT-25, 1975.

28. Jurewicz, J. T. and Stock, D. E., "A Numerical Model for Turbulent Diffusion in Gas-Particle Flows," ASME Paper No. 76-WA/FE-33, 1976.

29. Faeth, G. M., "Current Status of Droplet and Liquid Combustion," 1977 Spring Technical Meeting, Central States Section of The Combustion Institute, NASA Lewis Research Center, Cleveland, Ohio, 1977.

APPENDIX

EXPERIMENTAL RESULTS

Table 6

Spray Boundary Data, Noncombusting Methanol Jet

Pressure:	3 MPa	6 MPa		9 MPa	
z/d_o	r/r_o	z/d_o	r/r_o	z/d_o	r/r_o
10.3	1.9	9.7	2.9	10.0	3.8
20.6	3.7	20.3	5.0	20.4	6.7
30.9	4.5	30.1	6.7	30.2	9.5
41.2	6.7	46.5	8.6	40.2	11.4
51.6	8.3	50.8	11.3	51.3	16.2
61.9	11.1	61.2	14.9	61.3	19.9
71.5	13.3	71.4	16.8	71.4	22.3
82.5	18.0	82.3	19.8	81.8	25.0

Table 7

Spray Boundary Data, Noncombusting Pentane Jet

Pressure:	3 MPa	6 MPa		9 MPa	
z/d_o	r/r_o	z/d_o	r/r_o	z/d_o	r/r_o
10.1	3.9	10.2	4.9	10.0	3.5
20.6	6.2	20.1	5.6	20.0	6.6
29.9	7.9	36.4	8.4	30.0	8.0
41.6	9.6	41.0	12.0	40.2	12.9
51.8	13.0	51.2	14.9	51.5	15.2
61.4	14.9	61.1	16.7	61.6	17.6
71.6	15.6	71.4	19.0	71.4	19.9
82.3	17.5	81.6	20.2	81.8	21.1
92.7	18.5	91.8	21.3	92.8	23.5

Table 8

Spray Boundary Data, Combusting Methanol Jet

Pressure:	3 MPa	6 MPa		9 MPa	
z/d_o	r/r_o	z/d_o	r/r_o	z/d_o	r/r_o
11.4	3.8	13.3	5.0	13.1	12.3
43.0	8.2	43.0	10.2	42.8	11.5
71.8	12.5	73.1	13.6	72.9	14.6
104.9	12.6	104.0	15.1	104.2	0.0
142.3	0.0	132.4	0.0		

Table 9

Spray Boundary Data, Combusting Pentane Jet

Pressure:	3 MPa	6 MPa		9 MPa	
z/d_o	r/r_o	z/d_o	r/r_o	z/d_o	r/r_o
30.0	6.7	30.0	9.3	30.0	9.4
60.0	15.2	60.0	14.0	60.0	20.1
90.0	16.1	90.0	20.2	90.0	23.6
112.9	15.5	119.3	0.0	10.0	0.0
131.8	0.0				

Table 10

Flame Boundary Data, Methanol Jet

Pressure:	0.1 MPa	3 MPa		6 MPa		9 MPa	
z/d_o	r/r_o	z/d_o	r/r_o	z/d_o	r/r_o	z/d_o	r/r_o
14.9×10^3	115	15.0	12.8	15.0	14.0	15.0	15.6
30.0×10^3	135	45.0	22.2	45.0	37.3	45.0	29.2
49.8×10^3	203	60.0	25.5	60.0	32.8	60.0	34.9
59.8×10^3	155						
6.64×10^3	0.0						

Table 11

Flame Boundary Data, Pentane Jet

Pressure:	0.1 MPa	3 MPa		6 MPa		9 MPa	
z/d_o	r/r_o	z/d_o	r/r_o	z/d_o	r/r_o	r/d_o	r/r_o
$.89 \times 10^3$	246	30	10.4	30	13.4	30	14.5
1.59×10^3	433	60	18.5	60	24.7	60	25.8
1.63×10^3	588	90	25.3	90	40.6	90	41.7
3.44×10^3	650						
4.34×10^3	763						
5.35×10^3	700						
6.18×10^3	525						
7.06×10^3	338						
7.85×10^3	0.0						

REPORT DISTRIBUTION LIST

NASA-Lewis Research Center
Attn: Dr. R. J. Priem/MS 500-204
21000 Brookpark Road
Cleveland, OH 44135
(4 copies)

NASA-Lewis Research Center
Attn: Library/MS 60-3
21000 Brookpark Road
Cleveland, OH 44135

NASA-Lewis Research Center
Attn: Report Control Office/MS 5-5
21000 Brookpark Road
Cleveland, OH 44135

NASA-Lewis Research Center
Attn: E. A. Bourke/MS 500-205
21000 Brookpark Road
Cleveland, OH 44135

NASA Headquarters
Attn: RPS/Frank Stephenson
600 Independence Ave., SW, Rm. 526
Washington, DC 20546

NASA-Lewis Research Center
Attn: Procurement Section
Mail Stop 500-313
21000 Brookpark Road
Cleveland, OH 44135

NASA-Lyndon B. Johnson Space Center
Attn: EP/Joseph G. Thibodaux
Houston, TX 77058

NASA-George C. Marshall Space Flight Center
Attn: S&S-ASTN-PP/R. J. Richmond
Huntsville, AL 35813

NASA Scientific & Technical Information
Facility - Acquisitions Branch
P. O. Box 33
College Park, MD 20740 (10 copies)

Aerojet Liquid Rocket Company
Attn: David A. Fairchild
Bldg. 20001/Sec. 9732
P. O. Box 13222
Sacramento, CA 95813

Aerospace Corporation
Attn: Ellis M. Landsbaum
P. O. Box 92957
Los Angeles, CA 90045

Aerospace Corporation
Attn: Robert Doebler
2400 E. El Segundo Boulevard
Los Angeles, CA 90045

Air Force Rocket Propulsion Lab. (RPM)
Attn: Library
Edwards, CA 93523

Air Force Office of Scientific Research
Chief Propulsion Division
Attn: Dr. J. F. Masi (NAE)
Bolling Air Force Base
Washington, DC 20332

Air Force Rocket Propulsion Laboratory
Attn: Daweel George
Edwards, CA 93523

AFAPL
Research & Technology Div.
AF Systems Command
U. S. Air Force Commander
Attn: Frank D. Stull
Wright Patterson AFB, OH 45433

Air Force Rocket Propulsion Laboratory
Attn: Richard R. Weiss
Edwards, CA 93523

AFAPL
Attn: Frank D. Stull (RJT)
Wright Patterson AFB, OH 45433

Army Ballistics Research Labs.
Attn: Austin W. Barrows/DRDAR-BLP
Aberdeen Proving Grounds, MD 21005

Army Ballistic Research Labs.
Attn: Ingo W. May/DRDAR-BLP
Aberdeen Proving Grounds, MD 21005

Aeronautical Research Associates of
Princeton, Inc.
Attn: E. S. Fishburne
50 Washington Road
Princeton, NJ 08540

Army Material Command
Missile Systems Div.
Attn: Stephen R. Matos
Code AMCRD-MT
5001 Eisenhower Ave.
Alexandria,VA 22333

Air Force Systems Command
Arnold Engineering Development Center
Attn: Dr. H. K. Doetsch
Tullahoma, TN 37389

Aeronutronic Div. of Philco Ford Corp.
Technical Information Dept.
Ford Road
Newport Beach, CA 92663

Battelle Memorial Institute
Attn: Abbott A. Putnam
505 King Avenue
Columbus, OH 43201

Bell Aerosystems, Inc.
Attn: Library
Box 1
Buffalo, NY 14205

Bell Aerospace Company
Attn: T. F. Ferger
Post Office Box 1
Mail Zone, J-81
Buffalo, NY 14205

Bureau of Naval Weapons
Department of the Navy
Attn: Library
Washington, DC

Brooklyn Polytechnic Institute
Long Island Graduate Center
Attn: V. D. Agosta
Route 110
Farmingdale, NY 11735

California Institute of Technology
Jet Propulsion Laboratory
Attn: Fred E. C. Culick
204 Karman Lab
1201 E. California St.
Pasadena, CA 91109

California Institute of Technology
Jet Propulsion Laboratory
Attn: Raymond O. Kushida
4800 Oak Grove Drive
Pasadena, CA 91103

California State University, Sacrament
School of Engineering
Attn: Frederick H. Reardon
6000 J. Street
Sacramento, CA 95819

Chemical Propulsion Information Agency
Johns Hopkins University/APL
Attn: T. W. Christian
8621 Georgia Avenue
Silver Springs, MD 20910

Colorado State University
Attn: Charles E. Mitchell
Fort Collins, CO 80523

Frankford Arsenal
Attn: Martin Visnov
NDP-R, Bldg. 64-2
Bridge & Tacony Streets
Philadelphia, PA 19137

General Electric Company
Flight Propulsion Laboratory Dept.
Attn: D. Suichu
Cincinnati, OH 45215

Georgia Institute of Technology
School of Aerospace Engr.
Attn: Edward W. Price
Atlanta, GA 30332

Georgia Institute of Technology
Georgia Tech. Res. Inst.
Attn: Ben T. Zinn
Atlanta, GA 30322

General Electric Co.
Armament Systems Dept.
Attn: M. J. Bulman/Rm 1311
Lakeside Avenue
Burlington, VT 05402

Marquardt Corporation
16555 Saticory Street
Box 2013 - South Annex
Van Nuys, CA 91409

Melvin Gerstein
P. O. Box 452
Altadena, CA 91001

Institute for Defense Analysis
Attn: R. C. Oliver
400 Army-Navy Drive
Arlington, VA 22202

Johns Hopkins Univ./APL
Chemical Propulsion Information Agency
Attn: Thomas W. Christian
Johns Hopkins Road
Laurel, MD 20810

Commanding Officer
Army Research & Development
Command (ARRADCOM)
Attn: L. Stiefel/DRDAR-SCA-PE
Dover, NJ 07802

Massachusetts Institute of Technology
Department of Mechanical Engineering
Attn: T. Y. Toong
77 Massachusetts Avenue
Cambridge, MA 02139

McDonnell Douglas Corporation
McDonnell Douglas Astronautics Co.
Attn: William T. Webber
5301 Bolsa Avenue
Huntington Beach, CA 92647

D. E. Mock
Advanced Research Projects Agency
Washington, DC 20525

Lockheed Aircraft Corporation
Lockheed Propulsion Co., Div.
Attn: Norman S. Cohen
P. O. Box 111
Redlands, CA 92373

Naval Postgraduate School
Department of Aeronautics
Attn: David W. Netzer
Monterey, CA 93940

Naval Underwater Systems Center
Energy Conversion Dept.
Attn: Robert S. Lazar, Code 5B331
Newport, RI 02840

Naval Weapons Center Commander
Attn: Ronald L. Derr/Code 388
China Like, CA 93555

Naval Postgraduate School
Department of Aeronautics
Attn: Allen F. Fuhs
Monterey, CA 93940

Ohio State University
Department of Aeronautical and
Astronautical Engineering
Attn: R. Edse
Columbus, OH 43210

Chief Naval Research
Attn: James R. Patton, Jr/Code 473
800 N. Quincy Street
Arlington, VA 22217

Commander
Naval Surface Weapons Center
Attn: G. B. Wilmot
Silver Spring, MD 20910

Naval Weapons Center
Attn: Charles J. Thelen, Code 4505
China Lake, CA 93555

Propulsion Sciences, Inc.
Attn: Vito Agosta
P. O. Box 814
Melville, NY 11746

Princeton University
Forrestal Campus Library
Attn: Irvin Glassman
P. O. Box 710
Princeton, NJ 08450

Princeton University
Forrestal Campus Library
Attn: David T. Harrje
P. O. Box 710
Princeton, NJ 08540

Princeton University
Forrestal Campus Library
Attn: Martin Summerfield
P. O. Box 710
Princeton, NJ 08540

Purdue University
Jet Propulsion Laboratory
Project Squad
Attn: Robert Goulard
West Lafayette, IN 47907

Pennsylvania State University
Attn: Gerard M. Faeth
214 M. E. Building
University Park, PA 16802

Purdue University Res. Foundation
School of Mechanical Engineering
Attn: John R. Osburn
Thermal Sci. Propulsion Center Chaffee Hall
West Lafayette, IN 47906

Research and Development Associates
Attn: W. R. Espander
International Airport
ATO 9377
Albuquerque, NM 87119

Rockwell International Corporation
Rocketdyne Division
Attn: L. P. Combs, D/991-350
Zone 11
6633 Canoga Avenue
Canoga Park, CA 91304

Rockwell International Corporation
Rocketdyne Division
Attn: James A. Nestlerode/AB48
Dept. 596-124, AC46
6633 Canoga Ave.
Canoga Park, CA 91304

Rockwell International Corp.
Rocketdyne Division
Attn: R. C. Kesselring/AB48
6633 Canoga Ave.
Canoga Park, CA 91304

Rockwell Int. Corp. Rocketdyne Div.
Attn: Library Dept. 596-306
6633 Canoga Ave., Canoga Park, CA 91304

Susquehanna Corp.
Atlantic Research Div.
Attn: Library
Shirley Highway and Edsall Road
Alexandria, VA 22314

TISIA
Defense Documentation Center
Cameron Station, Bldg. 5
5010 Duke Street
Alexandria, VA 22314

Stanford Research Institute
333 Ravenswood Avenue
Menlo Park, CA 94025

Tennessee Technological University
Dept. of Mech. Engr.
Attn: Kenneth R. Purdy
P. O. Box 5014
Cookeville, TN 38501

TRW Systems, TRW, Inc.
Attn: A. C. Ellings
One Space Park
Redondo Beach, CA 90278

TRW Systems Group
STL Tech. Lib. Doc. Acquisitions
1 Space Park
Redondo Beach, CA 90278

Tulane University
Attn: J. C. O'Hara
6823 St. Charles Ave.
New Orleans, LA 70118

Science Applications, Inc.
Attn: R. B. Edelman/Suite 423
20335 Ventura Blvd.
Woodland Hills, GA 91364

Texas A & I University
Attn: Prof. James O'Hara
Civil & Mechanical Engr.
Kingsville, TX 78363

United Aircraft Corp.
Pratt & Whitney Div.
Florida Research & Development Center
Attn: Robert Carroll
P. O. Box 2691
West Palm Beach, FL 33402

Ultrasystems, Inc.
Attn: Thomas J. Tyson
500 Newport Center Dr.
Newport Beach, CA

United Aircraft Corp.
Pratt & Whitney Aircraft Div.
Attn: Thomas C. Mayes
P. O. Box 2691
West Palm Beach, FL 33402

United Aircraft Corp.
Attn: R. H. W. Waesche/MS20
400 Main Street
East Hartford, CT 06108

United Aircraft Corporation
United Technology Center
Attn: Library
P. O. Box 358
Sunnyvale, CA 94088

University of California
AErospace Engineering Dept.
Attn: F. A. Williams
Post Office Box 109
LaJolla, CA 92037

University of California, Berkeley
Dept. of Mechanical Engineering
Attn: A. K. Oppenheim
Berkeley, CA 94720

University of Illinois
Aeronautics/Astronautic Engr. Dept.
Attn: R. A. Strehlow
Transportation Bldg. Room 101
Urbana, IL 61801

University of Michigan
Attn: James A. Nicholls
P. O. Box 622
Ann Arbor, MI 48107

University of Utah
Dept. of Chemical Engineering
Attn: Alva D. Baer
Park Bldg. Room 307
Salt Lake City, UT 84112

University of Wisconsin, Mechanical Engineering Dept.
Attn: P. S. Myers
1513 University Ave.
Madison, WI 53706

United States Naval Research Lab.
Director (Code 6180)
Attn: Library
Washington, DC 20390

Virginia Polytechnic Institute State Univ.
Attn: J. A. Schetz
Blacksburg, VA 24061

Office of Assistant Director
(Chemical Technician)
Office of the Director of Defense
Research & Engineering
Washington, DC 20301